

An intercomparison of aerosol light extinction and 180° backscatter as derived using in-situ instruments and Raman lidar during the INDOEX field campaign

Sarah J. Masonis, University of Washington, Seattle, Washington, U.S.A.

Kathleen Franke, Albert Ansmann, Detlef Mueller, Dietrich Althausen, Institute for Tropospheric Research, Leipzig, Germany

John A. Ogren, Anne Jefferson, Patrick J. Sheridan, National Oceanic and Atmospheric Administration Climate Monitoring and Diagnostics Lab, Boulder, Colorado, U.S.A.

Abstract

Aircraft in-situ and Raman lidar profiles of aerosol light extinction (σ_{ep}) and 180° backscattering (β_p) are compared for days during the Indian Ocean Experiment (INDOEX). The measurements of σ_{ep} and β_p were made from the National Center for Atmospheric Research C-130 aircraft using two integrating nephelometers to measure light scattering and one Radiance Research Particle Soot Absorption Photometer to measure light absorption. Particulate 180° backscattering was measured in-situ using a new instrument, the 180° backscatter nephelometer. The Institute for Tropospheric Research Raman lidar was located on the island of Hulule (4.18N, 73.53E), and all of the in-situ profiles presented are from descents into the Hulule airport. Aerosol optical depth was also measured from Hulule using a sunphotometer and these data are included in the intercomparison. On average, the lidar-derived values of σ_{ep} and β_p are ~30% larger than the in-situ-derived values to a 95% confidence interval. Possible reasons for the overall discrepancy are: 1) a low bias in the in-situ measurements because of losses in the C-130 Community Aerosol Inlet; 2) underestimation of the humidification effect on light extinction in

the in-situ measurements; 3) overestimation of σ_{ep} and β_p in the lidar because of sub-visible cloud contamination; 4) errors in data processing that could be biasing either measurement, though the lidar retrievals are especially sensitive to this type of error. Temporal and spatial variability also appear to be the source of at least some of the discrepancy in two of the six cases, none of which are well collocated.

1.0 Introduction

Anthropogenically produced atmospheric aerosols are believed to have a significant effect on the radiative balance of the earth, particularly in highly polluted areas. In order to accurately calculate how aerosols affect climate the magnitude of this aerosol radiative forcing must be well quantified. This requires global mapping of both the horizontal and vertical distribution of aerosol optical properties.

Aerosol radiative forcing can be calculated using a combination of emissions estimates, chemical transport models (CTMs) and radiative transfer models. However, particularly in regions where there is a significant contribution to emissions by unregulated sources such as in India and Indonesia, emissions estimates are highly uncertain. These uncertainties are propagated through the CTM and radiative transfer calculations, wherein further uncertainty is added as each model must use simplified parameterizations of the chemical and physical interactions that actually occur in the atmosphere. Reliance on models alone is therefore not sufficient. Direct measurement of aerosol radiative properties is needed to accurately quantify the effect of aerosols on climate.

In recent years measurements of aerosol optical properties have been made both at long-term ground-based monitoring stations and in a series of intensive field campaigns. The monitoring stations and field campaigns often employ both in-situ measurement techniques as well as remote sensing techniques. Generally, in-situ measurement of light extinction by particles (σ_{ep}) is done by separately measuring its components, total light scattering (σ_{sp}) and light absorption (σ_{ap}). The former is usually determined using a nephelometer, which measures total scattering by aerosols, and the latter using a light absorption photometer, which measures light absorption by aerosols. It has recently become possible to also measure 180° backscattering by atmospheric aerosols (β_p) using a modified version of the TSI, Inc. nephelometer (Doherty et al., 1999).

When in-situ measurements are ground-based, assumptions about the vertical distribution and homogeneity of the aerosol are required in order to determine aerosol column optical depth. However when deployed in an aircraft these instruments can be used to measure optical properties throughout the vertical column of aerosol. In either case, simultaneous measurement of the aerosol size distribution and chemical properties is possible, allowing for a more complete characterization of the sampled aerosol than is possible using remote measurement techniques.

However, while in-situ measurements allow constraint of the optical properties of the aerosols present in the instrument's sample volume, these particles may or may not be representative of the aerosol that are actually present in the atmosphere. In particular, there may be inlet losses or the aerosol water content may change through heating or cooling of the sample. Remote measurement techniques do not suffer from these problems. The most reliable remote method of measuring total column optical depth is via sun photometer. These instruments are

widely deployed both at aerosol monitoring stations and during field campaigns. Some of the disadvantages of sun photometers are 1) they are only able to measure total column optical properties so vertical resolution is only attainable by mounting them on an aircraft and performing profiles, with the assumption that the atmosphere is invariant between the start and end of the profile; 2) in order to calculate aerosol extinction a cloud screening procedure must be part of the data processing and this screening may fail in certain cases, such as for sub-visible cirrus; 3) sun photometers do not separate RH effects from aerosol concentration effects.

Light detection and ranging (lidar) instruments are increasingly being employed to remotely measure atmospheric aerosols because the retrieved signal is highly resolved both vertically and temporally. As with sun photometers, the elastically backscattered lidar signal results from a combination of scattering by molecules, aerosols and clouds. A technologically advanced type of lidar, Raman lidar, can measure Raman-shifted backscattered light as well as elastically backscattered light. This allows for separation of molecular and particle backscatter returns and the determination of the particle backscatter coefficient (Ansmann et al., 1992a). Clouds are filtered out as part of the data processing algorithm using the lidar signal itself.

Aerosol optical properties derived from both the in-situ and remote techniques have some level of uncertainty. Theoretical exploration of uncertainty sources in each technique allow us to bound how well we know the derived quantities. However, it is possible that some sources of uncertainty may be underestimated or may be missed altogether in such an analysis.

Intercomparisons are useful because if they reveal discrepancies that fall outside the bounds of the respective measurement uncertainties then it is clear that one or more of the techniques

contains a source of uncertainty that is not sufficiently represented in the theoretical analysis or that there are data processing errors somewhere in the analysis.

Here we present such a case and explore some of the possible sources of disagreement. The measurements presented are from the Indian Ocean Experiment Intensive Field Phase (INDOEX IFP), which took place from February 16 through March 25, 1999. Profiles of light extinction and 180° backscatter as measured in-situ from an aircraft and remotely using a ground-based Raman lidar are compared. This was the first time that in-situ measurements of 180° backscatter have been made from an airborne platform. However, several other studies have presented comparisons of light extinction and/or aerosol optical depth as derived from aircraft in-situ and either ground- or aircraft-based sun photometers and lidar instruments. In the discussion section of this paper we compare our results with similar measurements made during the Tropospheric Aerosol Radiative Forcing Observational Experiment (Ferrare et al., 2000, Hartley et al., 2000) the Second Aerosol Characterization Experiment (Schmidt et al., 2000, Flamant et al., 2000) and at the Atmospheric Radiation Measurement Southern Great Plains site (Kato et al. 2000).

2.0 Field Site Measurements

During the INDOEX IFP in-situ measurements of total light scattering (σ_{sp}) and light absorption (σ_{ap}) were made by the Climate Monitoring and Diagnostics Lab of the National Oceanographic and Atmospheric Administration (NOAA-CMDL; Boulder, CO, U.S.A.). We made both ground and aircraft-based measurements but the data discussed herein is all from

instruments on board the National Center for Atmospheric Research (NCAR) C-130 aircraft based out of the island of Hulule in the Maldives (4.18N, 73.53E). The group used TSI, Inc. nephelometers to measure total light scattering at both low and high relative humidity at three wavelengths (450nm, 550nm, and 700nm) and a Radiance Research PSAP to measure light absorption at 550nm and low relative humidity.

Atmospheric aerosol 180° backscattering (β_p) was also measured from the C-130 aircraft by the University of Washington (UW; Seattle, WA, U.S.A.). This is the quantity directly sensed by a lidar instrument, so it is of particular interest when intercomparing in-situ and lidar measurements.

The INDOEX campaign was the first aircraft deployment of the 180° backscatter nephelometer. The instrument is a modified version of the TSI Inc. integrating nephelometer, whereby the lambertian white light source has been replaced with a 532nm laser. A complete description of the instrument is given by Doherty et al., 1999.

Remote measurements of atmospheric aerosols were made from the airport on the island of Hulule by the Institute for Tropospheric Research (IfT; Leipzig, Germany) using a multiwavelength lidar (Althausen et al., 2000) and an 18-channel sun photometer that was located on top of the lidar container, ~13.5m away from the lidar beam. The lidar measures elastic backscatter signals at six wavelengths and Raman backscatter signals at three wavelengths. The Raman signals from the IfT lidar are too weak to be detected in the presence of sunlight, and signals from nighttime observations must be averaged over between 30 minutes and 2 hours in order to reduce the statistical errors to tolerable values of 10 to 20%. When operated at night, the instrument can be used to derive 180° backscattering and light extinction

simultaneously and independently of each other. During the daytime the IfT lidar was used to measure β_p only.

2.1 Measurement collocation

The C-130 research flights generally took place from morning to early evening and in all cases the aircraft landed before dark. Thus the in-situ aerosol measurements were never simultaneous with the Raman lidar measurements of σ_{ep} , and the cases where measurements were close in time (within a few hours) are all from evening measurements. While the IfT Raman lidar cannot be used to retrieve σ_{ep} during daylight hours it can be used to retrieve profiles of β_p . These pre- and post-sunset profiles of β_p are used herein to check if there is a systematic change in aerosol scattering properties with time that would explain observed differences between the in-situ and lidar-derived profiles.

In addition to the problem of time coordination, the C-130 sometimes approached Hulule at a low altitude or conducted a slow descent with long horizontal legs built in, so we did not measure the vertical profile of aerosol over Hulule for all flights. Of a total of eighteen C-130 research flights we have identified six days where problems with each of the measurements of interest were minimized and the time/space difference between the C-130 descent into Hulule and IfT measurements was thought to be at a minimum (Figure 1 and Table 1). The latter requirement is aimed at reducing the possibility of spatial/temporal variability as a source of discrepancy between the two data sets.

The dates and times of these six measurement periods are given in Table 1, as are balloon sonde launch times. The sondes are used to retrieve atmospheric temperature and pressure profiles, which are used in the IfT lidar retrieval process; they are used to measure relative humidity profiles, which can be compared with the same as derived from the Raman lidar data. Table 1 also shows the times when IfT measured aerosol optical depth (AOD) at the Hulule airport using a sun photometer.

3.0 Data sampling and processing

3.1 In-situ data processing

All of the in-situ instruments measured air drawn into the aircraft via the NCAR C-130 Community Aerosol Inlet (CAI), but the measurements of light extinction and 180° backscatter were made on separate sample lines that were subject to different conditions. For the instruments measuring light extinction, aerosol drawn from the CAI were dried to 40-45% relative humidity (RH) and then were subjected to either a 1 μ m or 10 μ m diameter aerodynamic cut size. For all of the data discussed herein a 1 μ m diameter cut size was used. After measuring low-RH light scattering and light absorption the aerosol was re-humidified to 80-85% RH and light scattering was again measured. Details of the NOAA-CMDL hardware and methodology is presented by Sheridan et al. (2001).

The 180° backscatter nephelometer sampled air directly from the NCAR C-130 community aerosol inlet. The aerosol was neither subjected to a cut size nor to relative humidity

control, so β_p was measured at a relative humidity that varied with time and location. The measurement RH tracked the ambient RH but sometimes differed from ambient due to heating of the instrument and thermal inertia. Across the entire INDOEX campaign, the difference between the ambient and 180° backscatter nephelometer relative humidity was $20\% \pm 24\%$ RH.

The basic data processing algorithms for the in-situ measurements of light extinction are described in an accompanying paper (Sheridan et al., 2001). The in-situ 180° backscatter data are processed in a manner similar to that of the integrating nephelometer data; further details can be found in Doherty et al., 1999. In order to do a direct comparison between the remote and in-situ data sets we needed to make several adjustments to the in-situ data which are not described in the aforementioned references. These adjustments are described below.

The processed C-130 data are 4-second boxcar averaged, then the 180° backscatter data are further smoothed over a 12-second average window and the light absorption data over a 36-second averaging window. For the descent rates in the six profiles shown (Figure 1), a 4-second average corresponds, on average, to a vertical smoothing length of between about 10 and 30 meters. Data from horizontal legs are averaged to a single data point.

Sheridan et al. (2001) highlight several problems with the CMDL light extinction measurements that had to be rectified. We will briefly describe each, as their potential impact on the intercomparison will be discussed later. First, there were significant leaks in the light extinction instrumentation on some of the flights. Extensive laboratory testing showed that the leaks resulted in dilution of the sample air, so dilution correction factors have been used to compensate. The correction factor is never greater than 10% and has an altitude dependence such that it is zero at low altitudes (generally <1000m) where the pressure inside the instruments

exceeds than that of the aircraft cabin. Second, a system heater designed to dry the aerosol under very humid conditions sometimes caused particle volatilization. This heater was removed for the latter part of the campaign, and was not in place for three of days analyzed here (3/16/99, 3/21/99 and 3/25/99). As described by Sheridan et al., all data where heater-induced volatilization was apparent have been edited and so should not affect the results of this intercomparison. Finally, light absorption data are missing on two of the profiles (2/16/99 and 3/21/99), and there are no high-RH light scattering data for one of the profiles (3/16/99). We discuss below how we compensate for these missing data.

3.1.1 Adjustments made for this intercomparison

Wavelength matching

The Raman lidar primary wavelength is 532nm, as is the laser on the 180°-backscatter nephelometer. We have therefore adjusted light scattering and absorption at the measured wavelengths to that at 532nm using the following formulations:

$$\sigma_{\text{sp},532\text{nm}} = \sigma_{\text{sp},550\text{nm}} \left(\frac{550}{532} \right)^{\hat{a}(450/550)} \quad (1)$$

$$\sigma_{\text{ap},532\text{nm}} = \sigma_{\text{ap},550\text{nm}} \left(\frac{550}{532} \right) \quad (2)$$

where:

$$\hat{a}(450/550) = \frac{\log(\sigma_{\text{sp},450} / \sigma_{\text{sp},550})}{\log(550 / 450)}. \quad (3)$$

The wavelength dependence of light absorption is not well understood, but Eqn. 2 is consistent with theoretical and field studies (Foot and Kilsby, 1988). During INDOEX, $\hat{a}(450/550)$ was usually around 2 for polluted air, so this amounts to adjustments of about 7% to σ_{sp} and 3% to σ_{ap} .

Relative humidity adjustments

Light extinction and backscattering both change as an aerosol hydrates, so in order to make the in-situ and remotely-derived quantities comparable we have adjusted the measured values of σ_{sp} and β_p to ambient relative humidity. Total light scattering is measured at low (40-45%) and high (80-85%) relative humidity. We assume σ_s grows exponentially with relative humidity, then use the two measured values of total light scattering to calculate σ_{sp} at ambient relative humidity, as follows:

$$\sigma_{sp,ambientRH} = \sigma_{sp,meas} f(RH) \tag{4a}$$

where:

$$f(RH) = \left(\frac{100 - RH_{meas}}{100 - RH_{ambient}} \right)^\gamma \tag{4b}$$

and:

$$\gamma = \frac{\log(\sigma_{sp,highRH} / \sigma_{sp,lowRH})}{\log(100 - RH_{low}) / \log(100 - RH_{high})} . \tag{4c}$$

Light absorption is measured at low RH only, and it is not well understood how the light absorbing properties of aerosols change as particles hydrate. We therefore calculate light extinction as the sum:

$$\sigma_{\text{ep,ambientRH}} = \sigma_{\text{sp,ambientRH}} + \sigma_{\text{ap,lowRH}} \quad (5)$$

Using a low-RH value of light absorption for the in-situ calculation of light extinction clearly will lead to some error in the derived value of light extinction. The potential effect of this error on the comparison are discussed later.

Total light scattering was only measured at low RH (~40-45%) during Research Flight (RF) #13 on March 16. In order to convert the measured low-RH value of σ_{sp} to that at ambient relative humidity we must assume a value of $f(\text{RH})$ in Eqn. 4 above. During INDOEX the measured average value of $f(\text{RH})$ in going from 40-85% relative humidity was 1.6, taking into account only data for the central and northern Indian Ocean (north of 1°S latitude) and below 3km altitude (Sheridan et al., 2001). Therefore for RF#13 we have chosen to generate two profiles of σ_{sp} , one where we have set γ_{osp} to 0.189 and one where it is set to 0.424; these correspond to $f(\text{RH})_{40-85\%}$ values of 1.3 and 1.8 respectively.

As noted earlier, the in-situ measurement of 180° backscattering is made at a single RH. At times the instrument temperature is such that the measurement RH nearly matches that of the ambient air. However, when this is not the case we assume a functional fit as given in Eqn. 4. Because we do not measure β_{p} at low and high RH we cannot calculate the true value of $\gamma_{\beta_{\text{p}}}$ for the ambient aerosol, but Mie code can be used to establish a realistic range of values. In order to bound the possible range of values of β_{p} at ambient RH we have calculated two values of β_{p} for each profile. The first corresponds to a value of γ such that β_{p} at 85% RH is 1.2 times that at 40% RH, and the second profile corresponds to an increase in β_{p} of a factor of 2.5. When the difference between the measurement and ambient RH is large and/or when either relative

humidity is high (>85%) this correction factor will be large, leading to a high uncertainty in the derived value of β_p .

Missing light absorption data

Light absorption data are not available for the descent profile from RF #1 on February 16 and RF #16 on March 21. During INDOEX the average single scatter albedo ($\omega = \sigma_{sp} / (\sigma_{sp} + \sigma_{ap})$) of the aerosol in the north and central Indian Ocean for regions below 3km was 0.86 (Sheridan et al., 2001). We have therefore chosen to fill in the missing σ_{ap} data by generating two in-situ profiles corresponding to single scatter albedos of 0.75 and 0.9.

3.1.2 In-situ data uncertainty analysis

The instruments used for the in-situ measurements have each been calibrated and tested extensively in the laboratory using controlled sample streams, allowing for measurement uncertainties to be empirically determined (Anderson and Ogren, 1998, Bond et al., 1999, Doherty et al., 1999). However the measured quantity is not exactly the quantity of interest, in each case requiring some sort of adjustment (for example, from the measured relative humidity to ambient relative humidity). The in-situ data uncertainty analysis therefore also accounts for inaccurate conversion from the measured to the final parameter. Because σ_{sp} and σ_{ap} are measured independently we have separately determined their uncertainties; the total uncertainty in σ_{ep} is calculated by adding the two in quadrature. The uncertainty bounds given for the in-situ data reflect a 95% confidence interval.

For the in-situ values of total light scattering we include the following sources of uncertainty in the analysis: 1) instrument accuracy (7% of σ_{sp}); 2) calibration uncertainty ($\sim 1\%$ of σ_{sp}); 3) uncertainty in the adjustment of measured light scattering, which covers a range of scattering angles truncated in the forward and backward directions by $\sim 7-8^\circ$, to total light scattering ($\sim 1.4\%$ of σ_{sp} for the aerosol sizes measured during INDOEX); 4) instrument noise ($< 1\%-3\%$ of σ_{sp} for values of $\sigma_{sp} > 10 \text{ Mm}^{-1}$); 5) uncertainty in the adjustment of measured light scattering to σ_{sp} at ambient RH, caused by uncertainty in the humidification factor derived using Eqn. 4 above (set to 25% of the adjustment from σ_{sp} at 40-45% RH to σ_{sp} at ambient RH); 6) uncertainty in the wavelength-dependence of light scattering, used to convert from σ_{sp} at 550nm to σ_{sp} at 532nm (set to 50% of applied adjustment, or $\sim 3.5\%$); 7) uncertainty in corrections applied to account for leaks in the instrumentation ($\sim 0-6\%$ of σ_{sp} , but usually $< 2.5\%$ of σ_{sp} , for the profiles shown). Added in quadrature, these yield a total uncertainties of $\delta\sigma_{sp} \cong 8-9\%$ under dry (RH $< \sim 50\%$) conditions, but for an ambient RH of $\sim 90\%$ the uncertainty increases to $\sim 12\%$.

For the in-situ values of light absorption (σ_{ap}) we include the following sources of uncertainty in the analysis: 1) instrument accuracy (20% of σ_{ap}); 2) instrument precision (6% of σ_{ap}); 3) instrument noise (fixed at 1.64 Mm^{-1} for 36-second average); 4) uncertainty in an adjustment to the measured light absorption which accounts for signal amplification by light scattering (5-10% of σ_{ap}); 5) uncertainty in the wavelength-dependence of light absorption, used to convert from σ_{ap} at 550nm to σ_{ap} at 532nm ($\sim 3\%$ of σ_{ap}). Added in quadrature, these yield total uncertainties of $\delta\sigma_{ap} \sim 85\%$ for $\sigma_{ap} = 5 \text{ Mm}^{-1}$ and $\delta\sigma_{ap} \sim 30\%$ for $\sigma_{ap} = 25 \text{ Mm}^{-1}$. While these

uncertainties are quite large, recall that light extinction is dominated by light scattering, which has a much lower uncertainty.

Finally, for the in-situ values of 180° backscatter we include the following sources of uncertainty in the analysis: 1) instrument accuracy (10% of β_p); 2) uncertainty in the value used for the instrument calibration zero offset (fixed at $0.09 \text{ Mm}^{-1}\text{sr}^{-1}$); 3) uncertainty in the value used for the instrument calibration slope (16% of β_p); 4) instrument noise ($\sim 2\%$ - 14% of β_p for values of $\beta_p > 0.2 \text{ Mm}^{-1}\text{sr}^{-1}$); 5) uncertainty in the adjustment of measured light scattering to β_p at ambient RH, caused by uncertainty in the humidification factor derived using Eqn. 4 above (set to 100% of the adjustment from β_p at the measurement RH to β_p at ambient RH). If the applied humidification correction is small, the total uncertainty in β_p ($\delta\beta_p$) ranges from 68% for $\beta_p = 0.2 \text{ Mm}^{-1}\text{sr}^{-1}$ to 24% for $\beta_p = 2.0 \text{ Mm}^{-1}\text{sr}^{-1}$.

Because the humidification factor for β_p is unknown we calculate two profiles of in-situ-derived β_p for each intercomparison case. We set the lower uncertainty bound on the pair of profiles to $\beta_{p,\text{low } f(\text{RH})} - \delta\beta_p$ and the high uncertainty bound to $\beta_{p,\text{high } f(\text{RH})} + \delta\beta_p$. Similarly, where multiple profiles of light extinction are given because of missing light absorption or humidification factors we have set the lower and upper uncertainty bounds at the lowest and highest extreme values.

The uncertainty analysis described accounts for all known and quantifiable source of uncertainty in the in-situ measurements. However, the in-situ profiles of σ_{ep} and β_p may be biased by three unquantifiable sources of uncertainty: 1) aircraft aerosol inlet losses; 2) the

exclusion of aerosol with aerodynamic diameter $>1\mu\text{m}$ in the measurements of σ_{ep} ; 3) calculation of light extinction using a value of σ_{ap} measured at low-RH rather than at ambient RH.

3.2 Lidar Data Processing

Lidar instruments work by projecting a laser beam into the atmosphere and sensing laser light scattered into an angle of 180° , back towards the instrument. The intensity of the detected signal from a given altitude depends on 1) the power of the outgoing laser beam, 2) the amount of scattering material present at the altitude of interest, 3) the tendency of atmospheric components at the altitude of interest to scatter light into an angle of 180° versus other directions, 4) the amount of light loss along both the outgoing and return paths, and 5) the instrument calibration coefficients. The first and last of these can be characterized for any given instrument. The second quantity is generally the quantity of interest. The complication lies in disentangling 3) and 4). For a lidar that measures elastically scattered light only it is not possible to directly determine the profile of light extinction with altitude without knowing the ratio of light extinction to 180° -degree backscatter (known as the “lidar ratio”) for the atmospheric components at every point in the region of interest. The Raman lidar does not suffer from this fact.

Two signal profiles, the elastic and nitrogen Raman signal profiles, are measured by the instrument allowing us to retrieve profiles of the two unknowns, β_{p} and σ_{ep} , without a-priori knowledge of the aerosol lidar ratio. The inversion of the Raman lidar signal to derive 180° -backscatter and light extinction is described by Ansmann et al. (1990, 1992a). The profiles of σ_{ep} at 532nm that are presented herein are derived from the profile of the nitrogen Raman signal

measured at 607nm. The observed light extinction at this wavelength is the sum of the extinction along the outward propagating path at 532nm and extinction along the return path at 607nm. The measured value of σ_{ep} at 607nm is then converted to σ_{ep} at 532nm using a similar relationship to that given in Eqn. 1 above. The profiles of the backscatter coefficient, β_p , are derived from the ratio of the elastically scattered signal at 532nm and the nitrogen Raman signal at 607nm. In both cases, the profiles result from averaging over an hour of cloud-free data within the timeframes given in Table 1. The data are also averaged in the vertical, so that the profiles of β_p have a smoothing length of 180m and those of σ_{ep} 600m. Below we point out a few other aspects of the data processing algorithm that are germane to the intercomparison presented herein.

3.2.1 Factors in lidar retrievals that affect intercomparison

In order to determine aerosol extinction values below 3000m height with high accuracy the laser beam/receiver field-of-view overlap has to be known very accurately. The laser beam is transmitted into the atmosphere with a mirror that is mounted in such a way that the axis of the outgoing laser beam is co-located with the axis of the receiver field of view. Because of the transmitter configuration, the laser light cannot be detected by the receiver telescope in the lowest 250m. The portion of the laser beam seen by the telescope increases with distance from the lidar and is approximately 100% at about 3000m height. This overlap effect is described by the so-called overlap function. The overlap function can be experimentally determined from Raman lidar measurements when the atmosphere is almost particle-free above 800m (Wandinger and Ansmann, 2001). This was not the case during the INDOEX IFP, but it was the case during

the campaigns in July and October of 1999, when the overlap function was determined. Due to changes in the lidar adjustment the actual overlap function may slightly deviate from the one applied in the data evaluation. As a consequence, relative uncertainties in the correction of the overlap can be larger than 50% in the near-field range below about 800-1000m. Thus a proper determination of the particle extinction profile below 800-1000m is not possible.

To estimate the particle extinction coefficients in the lowest part of the troposphere the 180° backscatter profile is used. As mentioned earlier, β_p is calculated using signal ratios from the same view volume so the overlap effect is not a factor. The backscatter values are multiplied by an assumed lidar ratio to obtain the extinction coefficient. Here we have assumed a lidar ratio of 22.5sr, which is appropriate for marine aerosol particles according to both numerical studies (Ackermann, 1998) and our Raman lidar observations in clean marine environments. If you consider the full range of marine and continental aerosols present in the atmosphere 22.5sr is at the lower limit of the range of lidar ratios. In polluted layers where small, sometimes light absorbing, particles are present the lidar ratio increases to about 50-100sr. By using a low value for the lidar ratio in the near-surface retrieval the given values of σ_{ep} in this region represent minimum values of σ_{ep} .

3.2.2 Lidar data uncertainty analysis

Uncertainties for the lidar-derived values of σ_{ep} and β_p are discussed by Ansmann et al. (1992) and by Ferrare et al. (1998). Lidar-derived light extinction values are given for 532nm and have four significant sources of uncertainty, some of which vary with the magnitude of the determined extinction coefficient. The components of uncertainty and their approximate

magnitude for a range of σ_{ep} from 50-500 (Mm)⁻¹ are, for a 95% confidence interval: 1) uncertainty in the wavelength-dependence of light extinction at 532nm, which is the wavelength at which light extinction occurs between the lidar and the backscatter region, versus at 607nm, which is the wavelength at which light extinction occurs between the backscatter region and the lidar Raman sensing channel, (3% of σ_{ep}); 2) use of an incorrect profile of light extinction by Rayleigh scattering (via use of an incorrect air density profile), resulting in subtraction of the wrong amount of molecular scattering from the total measured extinction (0.3-2.0% of σ_{ep}); 3) error in the assumed laser-beam-receiver-field-of-view overlap function (4-30% of σ_{ep}); 4) error due to signal averaging (2-5% of σ_{ep}). As shown by Ansmann et al. (1992a), signal averaging leads to a mean extinction profile that corresponds to the mean atmospheric transmission properties. The mean extinction profile is related to the mean optical depth (as is desired) only if the optical properties are constant. As a consequence, signal averaging leads to an underestimation of the mean extinction coefficient if the aerosol optical properties vary. However, this underestimation is small if the measured profile is cloud-free. The total relative uncertainty due to systematic errors in the lidar-derived values of σ_{ep} , shown in Fig. 2a, is calculated by applying Gaussian's law of error propagation.

Raman lidar-derived values of β_p at 532nm have a similar set of uncertainty sources, with magnitudes given for a range of β_p from 0.5-5.0 Mm⁻¹-sr⁻¹: 1) uncertainty in the assumed reference value of the particle backscatter coefficient in the upper troposphere (i.e. an assumption of pure Rayleigh scattering), needed for calibrating the backscatter profile (5% of β_p); 2) use of an incorrect profile of light extinction by Rayleigh scattering via an incorrect air density profile (0.5-1.5% of β_p); 3) error due to neglecting the difference in particle transmission

at the laser wavelength of 532nm versus at the Raman wavelength of 607nm when evaluating the elastic-to-Raman signal ratio (2-5% of β_p); 4) error due to signal averaging (2-5% of β_p). Again, relative uncertainties as shown in Fig. 2b are calculated by applying the law of error propagation.

The uncertainty analysis given above applies to the values measured by the Raman lidar. Below ~1km we calculate σ_{ep} as the product of β_p and an assumed lidar ratio, so in this region we must calculate the uncertainty in σ_{ep} from the uncertainty in these two input parameters. Here we calculate the low bound on σ_{ep} as the product of the low bound on β_p (i.e. β_p minus its uncertainty) and 20, because 20 is at the very low end of the range of lidar ratios appropriate for atmospheric aerosols. The high bound on σ_{ep} is calculated as the product of the high bound on β_p and the average of the lidar ratio in the lowest 500m of the measured profile (i.e. ~1.0-1.5km). We use this approach because marine aerosols should be more prevalent below 1km than above it, driving the lidar ratio down. We therefore expect that the value of the lidar ratio between 1.0 and 1.5km is a realistic upper limit on the lidar ratio below 1km. For the six profiles shown, the lidar ratios used to calculate the high bounds on σ_{ep} are 29.5 (RF#1 on 2/16), 55.6 (RF#2 on 2/25), 69.9 (RF#9 on 3/07), 80.2 (RF #13 on 3/16), 81.2 (RF#16 on 3/21), and 71.3 (RF#18 on 3/25).

4.0 Results

4.1 Intercomparison between σ_{ep} and β_p from in-situ and lidar measurements

Profiles from the six comparison days are shown in Figures 3 through 8. Plotted for each day are both the lidar and in-situ derived values of light extinction (Figs. 3a-8a) and 180° backscatter (Figs. 3b-8b); the ratio of lidar-derived values to in-situ-derived values (Figs. 3c-8c); and the ambient relative humidity profiles associated with each measurement (Figs. 3d-7d). Show in figures 3a-8a and 3b-8b are both the in-situ and lidar data (circles, squares and plusses) and the uncertainty bounds on each. To calculate the ratios in Figures 3c-8c, the in-situ data, lidar data and sonde data were interpolated onto a 20m vertical grid. This has the effect of smoothing the data in some places, as well as providing common vertical spacing for each of the data sets. The relative humidity profiles (Figs. 3d-8d) and uncertainty bounds on the aerosol optical properties also show only the interpolated values.

For the six profiles presented two things are clear. First, the lidar measurements tend to give higher values of both σ_{ep} and β_p than do the in-situ measurements. Second, for altitudes above about 500m the two measurement techniques capture the same gross variations in σ_{ep} and β_p with altitude. Below 500m β_p is systematically higher in the lidar profiles; the large uncertainty in the lidar-derived value of σ_{ep} at these altitudes makes it difficult to know if this also holds true for light extinction.

4.1.1 Statistical analysis

To determine if there is indeed a systematic difference in the lidar and in-situ profiles and to explore the characteristics of the differences we have grouped the data from all six profiles together and done a statistical analysis. In Figure 9 we show the normalized differences between the lidar and in-situ measurements, which we calculate as:

$$\Delta\sigma_{ep} = \frac{\sigma_{ep,lidar} - \sigma_{ep,in-situ}}{\langle\sigma_{ep}\rangle} \quad (6a)$$

$$\Delta\beta_p = \frac{\beta_{p,lidar} - \beta_{p,in-situ}}{\langle\beta_p\rangle} \quad (6b)$$

where $\langle\sigma_{ep}\rangle$ and $\langle\beta_p\rangle$ are the averages of the lidar and in-situ values. The average normalized difference $\langle\Delta\sigma_{ep}\rangle$ and its 5-95% range, calculated only where $\sigma_{ep} \geq 10 \text{ Mm}^{-1}$ is 0.31 (-0.68 to 1.24), and $\langle\Delta\beta_p\rangle$, calculated only where $\beta_p \geq 0.2 \text{ Mm}^{-1}\text{sr}^{-1}$, is 0.36 (-0.52 to 1.05). Note that only data from $>1000\text{m}$ altitude were included in the calculation of $\langle\Delta\sigma_{ep}\rangle$ because of the large uncertainty in $\sigma_{ep,lidar}$ at lower altitudes.

The ratios given above were calculated using the central values of σ_{ep} and β_p shown in Figures 3-8, and all data – except σ_{ep} below 1000m – were included in the calculation. A stronger argument that there is a discrepancy between the two measurements comes from considering only those cases where the two measurements disagree beyond their uncertainty bounds, which happens 47% of the time for σ_{ep} and 42% of the time for β_p . Using these data only normalized differences were calculated as in Eqn. 6 above, where the central values of σ_{ep} and β_p were replaced with those *at* the uncertainty bounds. When the lidar value is higher than

the in-situ value the value at the lower lidar uncertainty bound and upper in-situ uncertainty bound was used in the calculation. When the lidar value is lower than the in-situ value, the higher lidar uncertainty bound and lower in-situ uncertainty bound were used to calculate the difference (Figure 10). The resulting average normalized differences, $\langle \Delta(\sigma_{ep} \pm \delta\sigma_{ep}) \rangle$ and $\langle \Delta(\beta_p \pm \delta\beta_p) \rangle$, yielded fractional differences of 0.29 (5-95% interval of -0.17 to 0.95) and 0.28 (95% interval of -0.28 to 0.82) respectively.

4.1.2 Case-by-case analysis

While, on average, the lidar data produce higher values of σ_{ep} and β_p there is variation in the discrepancies from one case to the next, and by looking at individual profiles we can gain insight as to possible sources for the overall discrepancy. On 2/16 there appears to be reasonable agreement between the two values of σ_{ep} , except between ~0.5km and 1.0km (Fig. 3a). The relative humidity plots (Fig. 3d) suggest that this difference may be due to difference in relative humidity in this regions. While the RH difference is not large aerosol hydration is very non-linear for RH above ~85%, as is the case for the in-situ profile. Unlike the σ_{ep} profiles the β_p data from 2/16 only agree within the measurement uncertainty bounds for about half of the profile and then only where the relative humidity is high and we assume a very large $f(\text{RH})$ for $\beta_{p,\text{in-situ}}$. The situation is similar for the data from 2/25 (Fig. 4) and 3/07 (Fig. 5), where disagreement in the profiles of σ_{ep} occur in regions of high relative humidity (this time during the lidar profile). Also we again see on 2/25 that there is little agreement between the two profiles of β_p , except where the ambient RH is high and we have assumed a large hydration

factor. The agreement is somewhat better on 3/7, where only a moderate hydration factor is needed for agreement in the central part of the haze layer (~0.3-1.3km). However, the very high relative humidity in this layer makes the uncertainty bounds on $\beta_{p,in-situ}$ so large that it would be difficult not to get agreement. In all three cases the most striking disagreement occurs below ~0.5km altitude, where the lidar-derived values of β_p increase dramatically near the surface. No such behavior was observed in the in-situ values of β_p at any time during the INDOEX campaign.

A somewhat different picture is seen on 3/16 (Fig. 6) where the profiles of light extinction have dissimilar shapes and the lidar clearly yields higher values. Above 1km the two only agree at the very top of the haze layer (where they converge to near zero extinction) and in a region just below 2000m. The agreement ~1.8-1.9km appears to be at least in part attributable to an enhancement in $\sigma_{ep,in-situ}$ associated with a sharp increase in relative humidity; this same peak in RH was not as evident during the lidar measurement. Unlike in the previous three cases, β_p shows better agreement on 3/16 than does σ_{ep} . However, the lidar values are still generally higher (factor of 1.2-2.0) for the central part of the haze layer. It is worth noting that on this day the in-situ value of β_p was measured at near-ambient RH for much of the profile so the humidification correction factor is very small, making $\beta_{p,in-situ}$ more well-constrained and providing a better comparison than on the previous three days.

The data from 3/21 (Fig. 7) stand out from the other five cases on two fronts: first, the haze layer varies dramatically in the vertical, and this variation is captured by both measurement methods; second, the two profiles of β_p appear to be largely in agreement above 1km. The in-situ values are in fact higher between about 2.4 and 3.2km than are the lidar values, possibly

because of a higher ambient RH during the in-situ measurements. Between 0.5 and 1.0km the uncertainty bounds on $\beta_{p,\text{in-situ}}$ are too large for a meaningful comparison, and below 0.5km there is again a dramatic increase in $\beta_{p,\text{lidar}}$ (and, accordingly, $\sigma_{\text{ep,lidar}}$) that is not present in the in-situ data. Also, below 2km the in-situ values of σ_{ep} again fall short of the lidar values in much the same way as on 3/16, and this does not appear to be attributable to differences in RH.

The profile on 3/25 (Fig. 8) shows the largest disagreement between the two methods. The two relative humidity profiles are nearly identical and the extinction and backscatter profiles have the same fundamental shape, indicating that the basic atmospheric structure did not change between the two measurement times. However, we do know that on this day the C-130 approached Hulule from the southeast (Fig. 1b) and that there was a significant north-south gradient in the pollution plume on this day. For altitudes >1000m the entire in-situ profile was taken more than 50km away from Hulule (Fig. 1a), so it may be that the enormous discrepancy on this day is due at least in part to a lack of collocation in the two measurements.

4.2 Intercomparison with aerosol optical depths from a sun photometer

Independent measurements of total column optical depth (τ) were made by IfT using a sun photometer. The data from these measurement are shown in Figure 11 along with the integrated optical depth as derived from the in-situ and lidar data. For the in-situ data we only present results for the three profiles where the measurements encompass a significant part of the haze layer (2/16, 3/16 and 3/21). Unfortunately we are lacking light absorption data on two of these days and are missing humidification information for σ_{sp} on the third, so we have calculated

two values of in-situ optical depth which correspond to the two profiles shown in Figures 3a, 6a and 7a. Also, only on 3/21 do the in-situ measurements encompass nearly the entire vertical extent of the haze layer, so for the other two days we calculated the full haze layer thickness by assuming a constant lidar ratio (on 2/16) or constant scattering (on 3/16) from the lowest altitude where we have data down to the surface. We also show two values of optical depth associated with the Raman lidar measurements. The first is the total optical depth (τ_{lidar}) and the second the optical depth only of aerosol above $\sim 1000\text{m}$ ($\tau_{\text{lidar},>1\text{km}}$), where it is possible for the Raman lidar to measure light extinction.

Assuming the actual aerosol optical depth does not change between the pre-sunset sun photometer measurement and the nighttime Raman lidar measurement, the difference between $\tau_{\text{lidar},>1\text{km}}$ and the sun photometer-derived optical depth indicates the amount of light extinction that is needed in the lower 1000m of the atmosphere to get agreement. It is clear from Fig. 12 that the bulk of the light extinction occurs in this region. Second, it is clear that, with one exception (3/25) the values of light extinction we have calculated for the lowest 1km of the atmosphere using a lidar ratio of 22.4 are too low to produce the optical depths needed to reach agreement with the sun photometer ($\tau_{\text{lidar},>1\text{km}}/\tau \sim 0.33$). For four of the six cases presented the optical depth in the lowest 1km would need to be about twice that shown in Figs. 3a-8a in order for agreement to be achieved. This implies that a lidar ratio of ~ 50 is a more appropriate value to use to calculate extinction in this region. This is consistent with the measured values of the lidar ratio above 1km during the INDOEX campaign.

The sun photometer measurements are always closer in time to the in-situ profiles than to the lidar profiles (Table 1), so in that sense they should be in better agreement with the in-situ

measurements. However, for the three cases for which we have data the in-situ optical depths are an average of 60% lower than the sun photometer values. For the three remaining days, given that the in-situ values of σ_{ep} tend to be lower than those from the lidar, it's likely that if we did have in-situ data from the full aerosol column the in-situ AODs for these days would be even lower than those from the lidar. This is clearly the case for 3/25 (Figure 8a).

While these arguments favor the lidar measurements over the in-situ measurements it is important to point out that achieving agreement between the lidar and sun photometer requires arbitrarily setting the lidar ratio to some value in the lowest 1km of the atmosphere, where the bulk of the light extinction occurs. Also, none of the three measurements were made on the same air mass, and both the lidar and the in-situ values of optical depth had to be calculated by employing a significant set of assumptions. It is therefore difficult to make robust conclusions from this intercomparison.

In a separate study, Bucholtz et al. (2001) compare differential optical depth as measured by the CMDL in-situ instruments versus the same as measured by a radiometer mounted on the outside of the C-130. This study shows good agreement between the two measurements at higher altitudes, but at lower altitudes the radiometer tended to measure larger values of AOD. The discrepancy in column-integrated optical depth was always less than ~30%. The authors believe this discrepancy may be explained in large part by the exclusion of coarse mode aerosol from the in-situ measurements, though it is unknown whether there was a significant coarse mode present during the intercomparison.

5.0 Discussion

The six cases presented indicate that the IfT Raman lidar produces values of light extinction and 180° backscatter that are ~30% higher than those given by the in-situ measurements to a 95% confidence interval. However, the lidar does not always produce higher values, especially at very high altitudes where the signal is smaller (Figure 10 and Figures 3-8). Possible explanations for the observed discrepancies fit into four general categories:

- 1) Problems with or bias in the in-situ measurements that systematically lead to underestimating both extinction and 180°-backscatter.
- 2) Problems with or biases in the lidar measurements that lead to overestimates of both extinction and backscatter.
- 3) Poor collocation of the two measurements.
- 4) An atmospheric phenomenon not presently understood that is sensed by the lidar but not by the in-situ measurements.

Of course, some combination of these four could be at play. Below we explore each of these possibilities, though we are unable to rule out any of the four categories at this time.

Other studies of a similar nature have also shown a discrepancy between aircraft in-situ values of light extinction and/or total aerosol optical depth relative to remote measurement methods. During the Tropospheric Aerosol Radiative Forcing Observational Experiment (TARFOX) Ferrare et al. (2000) found that in-situ aircraft measurements of light extinction were, on average, ~10% lower than ground-based lidar-derived values, although they note that this bias is within the uncertainties of the two measurements. Also using data from TARFOX,

Hartley et al. (2000) compare aerosol optical depth (AOD) as derived from the same in-situ instruments employed by Ferrare et al. with AOD as derived from an aircraft-based sun photometer. Again, on average the in-situ values are low by about 12%. They were unable to find a correlation between the discrepancy and the coarse mode fraction of the aerosol (which is always low), with ambient relative humidity, or with a number of other parameters. Ultimately they conclude the difference may be due to volatilization of aerosols in the in-situ measurements.

During the Second Aerosol Characterization Experiment (ACE-2), Schmidt et al. (2000) also compare in-situ aircraft-based measurements of AOD with those from an aircraft-based sun photometer. In this study the in-situ values were adjusted for the comparison by a scale factor between 1.04 and 4.9 to account for losses in the aircraft aerosol inlet. The resulting in-situ derived AOD for dust layers are biased relative to the sun photometer data by between +15% and -19% for one case and between -19% and -26% for a second case. The discrepancy for the AOD of the marine boundary layer is quite a bit higher: -13% to -23% for the first case and -20% to -44% for the second case. The authors do not put forth a reason for the bias, but they do note that very large correction factors were needed to account for inlet losses and so it is not surprising that closure was not always achieved.

In a study very similar to the one presented herein, Kato et al. (2000) compare aircraft in-situ measurements of sub-1 μm light extinction with σ_{ep} derived from a Raman lidar and they compare the in-situ AOD the same from a ground-based sun photometer. This study was based out of the Atmospheric Radiation Measurement Southern Great Plains (ARM-SGP) site in Oklahoma. The results are similar to those shown here, in that the lidar values of σ_{ep} are in general, but not always, higher than the in-situ values. The bias they observe is also similar in

magnitude to that seen here: the AOD derived from the sun photometer is ~28% higher than that derived from the in-situ measurements. They explore many of the same error sources that we investigate herein and conclude that the bias they observe is attributable to some combination of the following: 1) the use of a 1 μ m cut size in their in-situ measurements, 2) cloud contamination of the remote measurements, or 3) error in the adjustment of low-RH σ_{sp} measured on the aircraft to σ_{sp} at ambient RH, which is done using $f(RH)$ as measured using low- and high-RH nephelometers on the ground.

None of these studies is conclusive, but they do, as a collection, point to a relatively consistent discrepancy between in-situ and remote measurement methods. The data presented herein add further evidence of a bias in one or both measurements.

5.1 Explanation #1: Problems with or biases in the in-situ measurements

5.1.1 Exclusion of large aerosol from the in-situ measurements

The in-situ measurements were all made on aerosol brought into the aircraft via the C-130 Community Aerosol Inlet (CAI), and losses in the CAI may account for some of the discrepancy between the lidar and in-situ measurements. The CAI was not rigorously tested before the INDOEX experiment to determine particle losses, but it has recently been tested alongside a new Low Turbulence Inlet (LTI) which is designed specifically to pass larger diameter (>5 μ m) aerosol. The test results show that the CAI suffers from significant losses for coarse mode aerosol. However, the inlet does not have a sharp cutoff, and there is an

approximately linear decrease in the passing efficiency between $\sim 1\mu\text{m}$ and $7\mu\text{m}$, with a 50% cut point at between 3 and $4\mu\text{m}$ (Huebert et al., 2000).

It is also possible that the CAI is modifying the sampled aerosol via heating and cooling. Ram air heating will produce changes in the sample stream relative humidity and, if the heating is large enough, it could be causing particle volatilization. While this does not seem likely the inlet has not been rigorously tested for this effect so it is not possible to determine if it could be responsible for a significant decrease in optically relevant aerosol.

In addition to there being aerosol losses in the CAI, all in-situ light extinction measurements were intentionally made on aerosol that was subjected to a $1\mu\text{m}$ aerodynamic diameter cut size. If there was a significant super-micron aerosol component to the aerosol that passed through the CAI there would be a further systematic low bias to σ_{ep} . The aerosol sampled by the 180° backscatter nephelometer was not subjected to any cut size, so if this were the case than we would expect the discrepancies between the lidar and in-situ values of β_{p} to be smaller to some degree than those for σ_{ep} , which they are not.

5.1.2 Leaks in the instruments

As noted earlier, the instruments that measure light extinction had problems with leaks for part of the INDOEX campaign, and the data have been corrected to account for the resulting sample stream dilution. If the effect of the leaks was underestimated it could lead to a systematic underestimation in σ_{ep} . However, leaks are unlikely to be the source of the problem. The 180° -backscatter nephelometer system did not have large leak problems and profiles of β_{p} show similar discrepancies to those of extinction.

5.1.3 Particle volatilization in the light extinction measurements

Volatilization by the CMDL heating system is also unlikely to be the source of the problem, as there are large discrepancies even at altitudes where the relative humidity is low and the heater was not on. More to the point, the heater was not in place for three of the six flights presented (RF#13 on 3/16, RF#16 on 3/21 and RF#18 on 3/25). Finally, the 180-backscatter data exhibit large discrepancies and there was no heater on this system.

5.1.4 Accuracy of the nephelometers at measuring non-spherical aerosols

The integrating nephelometer does not actually measure total scattering, but instead measures integrating scattering from 7-170°. The measured value is then adjusted to total scattering using an angular truncation correction factor. This factor is a function of the aerosol size distribution but can be calculated using the ratios of scattering at the three wavelengths measured by the instrument. The correction factor increases with aerosol size, and in all cases the applied correction is appropriate for spherical aerosols. For non-spherical aerosol this angular truncation correction factor may be in error. However all of the profiles of σ_{ep} presented are from sub-1 μm size aerosol, and in this size range the angular truncation correction is small (<8%; Anderson and Ogren, 1998) so even if it was in error by a factor of two that would only result in a <4% error in derived scattering. Also, if this were the source of the discrepancy one would expect that there would be better agreement at higher relative humidity where the aerosol is hydrated and more nearly spherical, and this is not the case. In fact, the opposite is true (Figure 12).

A similar argument follows for the 180° backscatter nephelometer, which actually measures integrated 176°-178° scattering. Conversion to 180° backscatter is part of the instrument calibration, but this calibration is done using gases. We do not know how accurate the conversion is for non-spherical aerosol. We do know that for spherical aerosol 176°-178° scattering is an excellent proxy for β_p , agreeing to within ~2% for aerosol size distributions in the sub-1 μ m range aerosol and within ~10% for aerosol size distributions ~1-5 μ m (Doherty et al., 1999) so the adjustment to the measured value is very small. In order for aerosol non-sphericity to be the source of the discrepancy in β_p the difference between integrated 176°-178° scattering and 180° scattering would have to be systematically a great deal larger for irregularly shaped aerosol than for spherical aerosol.

5.1.5 Underestimation of aerosol hydration effects

It is possible that the in-situ measurement is systematically underestimating the increase in aerosol total light scattering with RH. Light scattering is measured at low and high RH by drying then re-hydrating the aerosol. If the residence time in the humidification system is not long enough for the aerosols to become fully hydrated then the high-RH measurement will be too low. This “kinetic effect” should only cause large errors at higher RH and the effect should increase with RH. Figure 12a shows that $\langle \Delta\sigma_{ep} \rangle$ is about zero at low relative humidity and that there is a small but statistically significant correlation between the normalized difference in light extinction and the average RH ($r=0.41$, $0.07 \leq r \leq 0.67$ 95% C.I.). This can account for about half of the noted discrepancy in σ_{ep} ($r^2=0.17$). We have not plotted RH versus $\langle \Delta\beta_p \rangle$ because for

most of the profiles β_p can assume a large range of values, depending on the assumed humidification factor, so the correlation would not be meaningful.

5.1.6 Underestimation of light absorption via hydration effects

Light absorption is measured at low (40-45%) RH. Some people have argued that light absorption could be magnified considerably in humidified aerosol where the light absorbing component is in the core (Fuller, 1995). The magnification effect is caused by multiple scattering within the aerosol. This could mean there is a low bias in the light extinction data which would increase with relative humidity. Such an effect would also explain the correlation between $\langle \Delta\sigma_{ep} \rangle$ and RH. In order for this effect to fully account for this correlation σ_{ap} would have to approximately double with hydration. However, we do not at this time have a way of exploring this possibility.

5.2 Explanation #2: Problems with the lidar measurements

The lidar instrument by nature measures the ambient aerosol so there is no concern that some of the aerosol may be missed or that it is somehow perturbed by the measurement itself as there is in the case of in-situ measurements. Errors in the lidar data therefore would result from either errors in the data processing or in the instrument calibration.

5.2.1 Errors in data processing

The uncertainty bounds given in Figures 3-8 account for all known sources of uncertainty, but are only appropriate if there are no errors in the data processing routines. Both the in-situ and lidar-derived profiles are of course subject to data processing errors. However, the lidar-retrieved values of σ_{ep} and β_p are much more sensitive to plausible data processing errors than are the in-situ data. This was clearly demonstrated to us in the course of preparing this paper, when it was realized that errors in how the overlap correction factor had been applied and reasonable adjustments to the system calibration resulted in profiles of σ_{ep} and β_p that were up to a factor of three larger than those shown in Figures 3-8. One of the erroneous profiles – the corrected version of which is presented herein (3/25) – was published before these errors were corrected (Ansmann et al., 2000). As part of this intercomparison, the data processing algorithms have been carefully scrutinized multiple times, and it is highly unlikely that significant data processing errors remain.

5.2.2 Alignment changes

Derived values of light extinction are very sensitive to changes in the applied laser-beam/field-of-view overlap correction factor. This correction factor changes with system alignment and can only be determined by making measurements while the atmosphere is essentially particle-free above ~800m. While the atmosphere was never clean during the INDOEX Intensive Field Phase the lidar was run at other times of the year when observations could be made on pristine air from the southern hemisphere. Data from these times were used to determine the system overlap function. In the lidar uncertainty analysis we account for how

changes in the adjustment of the system optics would affect the retrieved value of σ_{ep} by allowing the overlap correction factor to vary by its full range of measured values over the past two years. It is possible that the system alignment changed systematically between the INDOEX IFP and the time when the overlap correction function was determined by a larger amount than is accounted for in the uncertainty analysis. If this were the case it would lead to either a high or low bias in σ_{ep} , especially at lower altitudes. However, the lidar system alignment is checked about once a week using a fixed alignment procedure, so it seems very unlikely that the alignment would be in error during the entire INDOEX IFP and that this would not have been noticed.

5.2.3 Cloud contamination of lidar data

The lidar data shown have been averaged over both space (vertically) and in time. Each profile is comprised of one hour of data, but the data chosen are not always contiguous. The data are carefully examined for cloud contamination and only profiles that are believed to be cloud-free are included in the average. The lidar signal magnitude, spatial variability and temporal variability are used to determine if clouds are present. However, it is possible that the lidar profiles have some cloud contamination. Sub-visible small-scale intermittent “wafts” of cloud could bias the lidar signal high.

If this is the case, we would expect the discrepancies to be higher in regions of higher relative humidity which, as we have shown earlier, is indeed the case. In addition, time-height plots of the backscattered return signal show that clouds were more frequently present after sunset than before, increasing the chances for cloud contamination.

5.3 Poor collocation of the two measurements

As noted earlier, the Raman lidar runs were all made after dark and the C-130 aircraft always landed before dark. Therefore there is always a gap between the in-situ and lidar measurements of ~1-3.5 hours. In fact we see that of the six cases presented we get the largest discrepancies on 3/16, when the two measurements had the largest time separation, and on 3/25, when we know that the aerosol was highly variable both temporally and spatially.

Atmospheric conditions can change between day and night, and in particular the relative humidity can increase at night as the air cools. Light scattering properties increase as relative humidity increases, so this is clearly a candidate for explaining the observed discrepancies. In order to explore this possibility we have shown the relative humidity profiles taken in coordination with each measurement (Figures 3d-8d). While in some cases the profiles do show differences there is no clear bias towards higher relative humidity around the time of the lidar measurements. However, there is a very small but statistically significant correlation between discrepancies in σ_{ep} and the difference in the RH taken from the sondes (which were coordinated with the lidar runs) and the RH as measured on the C-130 (Figure 11b; $r=0.269$, $0.02 \leq r \leq 0.57$ 95% C.I). This explains <25% of the noted discrepancy between the lidar and in-situ values. In addition, the sonde measurements were not made at exactly the same time as the lidar measurements, nor are they perfectly co-located in space. There is therefore some uncertainty in how well the RH profile from the sonde corresponds to the lidar data. When this is accounted for the noted small correlation probably becomes statistically insignificant.

While the IfT Raman lidar cannot be used in daylight to derive profiles of light extinction it is possible to use the elastically backscattered signal to derive profiles of β_p at the time the in-situ profile was made. This is accomplished by applying the Klett inversion method (Klett, 1985) and assuming that the lidar ratio is unchanged between the time of the C-130 profile and the nighttime lidar measurements (Figure 13). These data also do not indicate any sort of systematic increase in β_p between the time of the in-situ and lidar measurements. For three of the days (3/07, 3/21 and 3/25) the profiles of β_p are nearly identical, and on 2/16 and 2/25 β_p is about the same or, at some altitudes, larger at the time of the in-situ measurements than during the Raman measurements. The one exception is on 3/16, where β_p is systematically lower at the time of the C-130 landing. This could explain at least part of the particularly large discrepancy on this day.

The case of 3/25 is striking because atmospheric variability is our leading hypothesis for the very large discrepancy seen on this day, yet there is no apparent change in β_p . However, the comparison in Fig. 13 only accounts for the temporal atmospheric variation, not spatial variation. A strong north-south gradient in the haze layer, as was observed from the C-130 aircraft, could still result in the discrepancies we see in Figure 8.

The fact that for five of the six profiles there is not a systematic increase in β_p with time means that, unless the lidar ratio always increases at night, there also should not be a systematic increase in σ_{ep} . With no apparent change in air mass or tendency for relative humidity to systematically increase or decrease it is unlikely that the lidar ratio somehow increases with time.

5.4 A phenomenon not presently understood

Here we give an example of a condition that could lead to the noted discrepancy but which is not currently well-understood. Of course by definition this category consists of other similar phenomena that we just haven't yet discovered or thought to consider.

It is possible that we have not fully considered the effect of clouds on aerosol optical properties. Time series from the Raman lidar sometimes show enhanced backscatter and extinction *after* clouds have passed overhead. During these times there were no clouds visible by eye and there was no sharp increase in the lidar signal to indicate the presence of a cloud base. The common thinking is that clouds are readily distinguished from aerosols due to droplet activation causing a step change in scattering. However, this applies only to the cloud-formation process; there is no comparable step-change on the evaporation side. Thus, tenuous evaporating clouds that slowly dissipate into the clear-sky aerosol could lead to enhanced scattering. This would certainly lead to an enhancement in the lidar profiles of σ_{ep} and β_p , but it would probably have the opposite effect on the in-situ measurements. This is because aerosol that has been cloud-influenced as described would be enlarged by hygroscopic growth and thus would have a lower passing efficiency in the C-130 CAI.

6.0 Conclusions

Independent measurements of light extinction and 180° backscatter using in-situ instruments and a Raman lidar reveal a significant difference in the derived quantities. On

average, the lidar yields values of σ_{ep} that are ~30% higher to a 95% confidence interval. The fact that a large discrepancy exists between the two data sets indicates that either the two platforms are measuring different things – because of real atmospheric variability or because one or both of the instruments are not measuring all of the aerosol and *only* aerosol – or that the uncertainty bounds on one or both of the data sets does not appropriately reflect the true uncertainty in the measurement. Poor collocation of the profiles does not allow us to decisively separate these two possibilities. Interpretation of the result would also be easier if the uncertainty bounds on β_p and σ_{ep} could be reduced. In particular, our lack of knowledge of the relative humidity dependence of β_p means that the uncertainty bounds on the in-situ profiles are often so large that the intercomparison is not very meaningful.

Nonetheless, because we have an ensemble of intercomparison profiles and because we have applied confidence intervals to the profiles we feel that our conclusion that there is a systematic difference between the two measurement methods is robust. It is also important to note that if we had only one intercomparison profile the conclusions of this study might have been quite different. For example, the profiles on 3/21 (Fig. 6) alone would lead to the conclusion that there is reasonably good agreement, whereas the profiles on 3/25 (Fig. 8) would give the opposite conclusion. In addition, by having an ensemble of cases we are able to reach some conclusions about possible sources of the discrepancy using statistical analysis.

While we cannot state definitively the source of the discrepancy, we can list the most likely candidates. First, we know that the C-130 Community Aerosol Inlet does not perfectly transmit the ambient aerosol into the sensing volumes of the in-situ instruments. Recent test of the CAI indicate that there were significant losses even in the sub-1 μ m size range and that losses

became dramatic above 2-3 μm . However, a lack of information on the ambient aerosol size distributions makes it difficult to accurately quantify the potential magnitude of this effect. The use of a 1 μm aerodynamic cut size in the light extinction measurements may also be biasing the in-situ values of σ_e somewhat low, but the CAI tests indicate that most of the coarse mode aerosol is lost in the inlet, so the impactor probably has little effect. This is evidenced by the fact that the discrepancies between the lidar and in-situ values of β_p are about the same as those for σ_{ep} , and the in-situ measurements of β_p were made on the full aerosol that came in the CAI.

Second, we see that there is a moderate but significant correlation between the ambient relative humidity and normalized differences in the two measurements (Fig. 11). This points to three possibilities: 1) underestimation of the humidification effect on light extinction in the in-situ measurements, 2) overestimation of σ_{ep} and β_p in the lidar because of sub-visible cloud contamination, and 3) losses in the C-130 Community Aerosol Inlet which are enhanced at high relative humidity because of the increase in aerosol diameter with humidification. At this time we do not have the information needed to distinguish between these possibilities. As noted earlier, humidification effects and/or cloud contamination can only account for about half of the observed discrepancy.

Temporal and spatial variability provide a third plausible explanation. It seems likely that this accounts for at least some of the discrepancy on 3/16, where we see that β_p , and therefore probably also σ_{ep} , increased systematically between the time of the in-situ measurement and the time of the Raman lidar measurement (Figs. 6 and 13). On 3/25 we do not see a change in backscattering with time, but we do know that on this day the aerosol had a large north-south gradient. The C-130 approached Hulule from the southeast and entered the top of

the haze layer ~100km from the airport; at 1km altitude it was still ~50km from the lidar site (Fig. 1). Spatial variability thus could be causing some or all of the observed discrepancy on this day. However, on average, β_p does not appear to systematically increase with time (Fig. 13) so temporal variability cannot explain the discrepancies seen in the ensemble of six profiles. Nor is it likely that spatial variability is to blame, as the aircraft approached the airport from a variety of directions (Fig. 1b) so spatial variations, even if they are consistent with time, should result in randomly distributed errors.

Fourth, we cannot exclude the possibility that data processing errors could be biasing either or both of the data sets. The Raman lidar is particularly sensitive to these types of errors, though as part of this intercomparison the data processing routines have been carefully scrutinized several times and are unlikely to contain significant mistakes.

Finally, the discrepancy could be due in part to an atmospheric phenomenon that we do not yet understand. One example would be the slow evaporation of water from aerosols that have passed through clouds. These aerosol would be more hydrated than ambient relative humidity conditions indicate, but would not be hydrated enough to be flagged as “cloud contaminated” in the lidar data. Such aerosol might be excluded by the C-130 CAI because of its larger size.

Acknowledgements

This research was funded through the National Science Foundation Climate Dynamics Program (Grant #ATM-9612888), the Office of Naval Research (Grant #N00014-98-1-0809), and the National Oceanic and Atmospheric Administration via the Joint Institute for the Study of

the Atmosphere and Oceans under agreement NA67RJ0155, contribution #799. Additionally, we thank NSF for providing C-130 flight hours for the INDOEX IFP and the NCAR Research Aviation Facility for conducting a safe and well-organized field deployment. Thanks are also due to Tony Clarke, Tad Anderson and David Covert for helpful discussions about the data.

References

Ackermann, J., The extinction-to-backscatter ratio of tropospheric aerosol: a numerical study, *J. Atmos. Ocean. Tech.*, 15, 1043-1050, 1998.

Althausen, D., D. Müller, A. Ansmann, U. Wandinger, H Hube, E. Clauder, and S. Zörner, Scanning, 6-wavelength, 11-channel aerosol lidar, *J. Atmos. and Oceanic Technol.*, 17, 1469-1482, 2000.

Anderson, T. L., D. S. Covert, S. F. Marshall, M. L. Laucks, R. J. Charlson, A. P. Waggoner, J. A. Ogren, R. Caldow, R. L. Holm, F. R. Quant, G. J. Sem, A. Wiedensohler, N. A. Ahlquist, and T. S. Bates, Performance characteristics of a high-sensitivity, three-wavelength, total scatter/backscatter nephelometer, *J. Atmos. Oceanic Tech.*, 13, 967-986, 1996.

Anderson, T. L., and J. A. Ogren, Determining aerosol radiative properties using the TSI 3563 integrating nephelometer, *Aerosol Sci. Technol.*, 29, 57-69, 1998.

Ansmann, A., M. Riebesell, and C. Weitkamp, Measurements of atmospheric aerosol extinction profiles with a Raman lidar, *Opt. Letts.*, 15, 746-748, 1990.

Ansmann, A., M. Riebesell, U. Wandinger, C. Weitkamp, E. Voss, W. Lahmann, and W. Michaelis, Combined Raman elastic-backscatter lidar for vertical profiling of moisture, aerosol extinction, backscatter, and lidar ratio, *Appl. Phys. B*, 55, 18-28, 1992a.

Ansmann A., U. Wandinger, M. Riebesell, C. Weitkamp, and W. Michaelis, Independent measurement of extinction and backscatter profiles in cirrus clouds by using a combined Raman elastic-backscatter lidar, *Appl. Opt.*, 31, 7113-7131, 1992b.

Ansmann, A., D. Althausen, U. Wandinger, K. Franke, D. Müller, F. Wagner, and J. Heintzenberg, Vertical profiling of the Indian aerosol plume with six-wavelength lidar during INDOEX: A first case study, *JGR*, 27, 963-966, 2000.

Bond, T. C., T. L. Anderson, and D. Campbell, Calibration and intercomparison of filter-based measurements of visible light absorption by aerosols, *Aerosol Sci. Technol.*, 30, 582-600, 1999.

Bucholtz, A., P. J. Sheridan, J. A. Ogren, D. Baumgardner, and F. P. J. Valero, A comparison between direct airborne radiometric measurements of visible aerosol optical depth and nephelometer derived values during INDOEX, *JGR*, this issue.

Doherty, S. J., T. L. Anderson, and R. J. Charlson, Measurement of the lidar ratio for atmospheric aerosols with a 180° backscatter nephelometer, *Appl. Opt.*, 38, 1823-1832, 1999.

Ferrare, R. A., S. H. Melfi, D. N. Whiteman, K. D. Evans, and R. Leifer, Raman lidar measurements of aerosol extinction and backscattering: 1. Methods and comparisons, *JGR*, *103*, 19663-19672, 1998.

Ferrare, R., S. Ismail, E. Browell, V. Brackett, S. Kooi, M. Clayton, P. V. Hobbs, S. Hartley, J. P. Veefkind, P. Russell, J. Livingston, D. Tanré, and P. Hignett, Comparisons of LASE, aircraft and satellite measurements of aerosol optical properties and water vapor during TARFOX, *JGR*, *105*, 9935-9947, (2000).

Foot, J. S. and C. G. Kilsby, Absorption of light by aerosol particles: an intercomparison of techniques and spectral observations, *Atmos. Env.*, *23*, 489-495, 1989.

Fuller, K. A., Scattering and absorption cross sections of compounded spheres. III. Spheres containing arbitrarily located spherical inhomogeneities, *J. Opt. Soc. Am. A*, *12*, 893-904, 1995.

Hartley, W. S., P. V. Hobbs, J. L. Ross, P. B. Russell, and J. M. Livingston, Properties of aerosols aloft relevant to direct radiative forcing off the mid-Atlantic coast of the United States, *JGR*, *105*, 9859-9885, (2000).

Huebert, B. A., S. G. Howell, D. Covert, A. Clarke, J. R. Anderson, Passing Efficiency of a Low Turbulence Inlet (PELTI): Final Report to NSF, 13 Sept. 2000.

Kato, S., M. H. Bergin, T. P. Ackerman, T. P. Charlock, E. E. Clothiaux, R. A. Ferrare, R. N. Halthore, N. Laulainen, G. G. Mace, J. Michalsky, and D. D. Turner, A comparison of the aerosol thickness derived from ground-based and airborne measurements, *JGR*, *105*, 14701-14717, (2000).

Schmid, B. J. M. Livingston, P. B. Russell, P. A. Durkee, H. H. Johnsson, D. R. Collins, R. C. Flagan, J. H. Seinfeld, S. Gasso, D. A. Hegg, E. Öström, K. J. Noone, E. J. Welton, K. J. Voss, H. R. Gordon, P. Formenti, M. O. Andreae, Clear-sky closure studies of lower tropospheric aerosol and water vapor during ACE-2 using airborne sunphotometer, airborne in-situ, space-borne, and ground-based measurements, *Tellus*, *52B*, 568-593, (2000).

Sheridan, P. J., A. Jefferson, and J. A. Ogren, Spatial variability of aerosol optical properties over the Indian Ocean during INDOEX, *JGR*, submitted, (2001).

Wandinger, U. and A. Ansmann, Experimental determination of the lidar overlap profile with Raman lidar, *Appl. Opt.*, submitted (2001)

TABLE 1

Date	research	Profile times (UTC):			
	flight #	in-situ	lidar	sonde launch	sun photometer
2/16	RF #1	14:33-14:54	15:17-16:22	13:59	11:30
2/25	RF #5	12:35-13:00	14:18-15:52	12:16	12:00
3/07	RF #9	12:23-12:58	14:58-16:17	11:18&15:04	12:08
3/16	RF #13	11:23-11:31	14:40-15:40	12:33&16:01	11:40
3/21	RF #16	12:05-12:13	13:43-14:53	08:55 & 14:36	12:20
3/25	RF #18	13:00-13:16	13:30-15:00	14:33	12:00

Figure Captions:

Figure 1: The C-130 aircraft distance from Hulule airport during the profiles used in this intercomparison. Note that data from horizontal legs are averaged across the leg.

Figure 2: Fractional uncertainties used for the IFT Raman lidar values of light extinction and 180° backscatter.

Figures 3-8: Intercomparison plots for Research Flight (RF) #1 on February 16, 1999.

- a) Lidar (blue plusses) and in-situ (red circles & pink squares) derived values for light extinction. Low and high uncertainty bounds (95% C.I.) for both are also shown. Light absorption was not measured on this profile, so pink squares correspond to an assumption of single scatter albedo = 0.75, and red circles to an assumption of single scatter albedo = 0.90.
- b) As in a), only for 180° backscatter. Here the red circles correspond to an assumed $f(\text{RH})$ for β_p of 1.2 and the pink squares correspond to an assumed $f(\text{RH})$ of 2.5.
- c) The ratio of lidar-derived values to in-situ derived values. Light extinction ratios are shown in pink and red (thin and thick lines) and 180° backscatter values in blue and green (dashed and dotted lines).
- d) The relative humidity profiles from the in-situ measurements (thick red line) and from the sonde(s) launched in coordination with the lidar run (thin blue line). Where more than one sonde was launched we show profiles from both (solid and dashed blue lines).

Figure 4: As in Figure 3, but for RF#5 on February 25, 1999.

Figure 5: As in Figure 3, but for RF#9 on March 7, 1999.

Figure 6: As in Figure 3, but for RF#13 on March 16, 1999. Light scattering was only measured at low RH for this profile, so in a) the red circles correspond to an assumption of $f(\text{RH})=1.3$ for light scattering and the pink squares to $f(\text{RH})=1.8$ for light scattering. The humidification factor

$f(\text{RH})$ is defined as the fractional change in light scattering in going from 40% to 85% relative humidity.

Figure 7: As in Figure 3, but for RF#16 on March 21, 1999. As in Figure 3a, the pink squares correspond to an assumption of single scatter albedo = 0.75, and red circles to an assumption of single scatter albedo = 0.90.

Figure 8: As in Figure 3, but for RF#18 on March 25, 1999.

Figure 9: The normalized difference in between the lidar and in-situ values of (a) light extinction and (b) 180° backscatter versus altitude (Eqn. 6).

Figure 10: As in Figure 9, but using only data where the two measurement techniques disagree within a 95% confidence interval. Here the differences are calculated using the values of (a) σ_{ep} and (b) β_{p} at the two closest uncertainty bounds.

Figure 11: Total column aerosol optical depth for the six intercomparison days, as measured by in-situ instruments (triangles), Raman lidar (open squares) and a sun photometer (solid dots). The in-situ and lidar values are calculated by integrating the light extinction profiles shown in Figures 3-8. The in-situ profiles of light extinction on February 25 and March 7 only covered a small portion of the haze layer, so we have not calculated optical depth for these days. We also show the integrated optical depth from the Raman lidar using only the portion of the profile above 1km, where extinction is actually measured (squares with x's through them).

Figure 12: The normalized difference in light extinction versus (a) the average relative humidity of the in-situ and lidar profiles and (b) the difference in the lidar and in-situ RH profiles. Note that data are only shown for values of σ_{ep} above 1km.

Figure 13: A comparison of lidar-derived 180° backscatter as shown in Figures 3b-8b (blue solid lines) and as derived using the Klett method at the time of the in-situ profile measurements (green dashed lines).

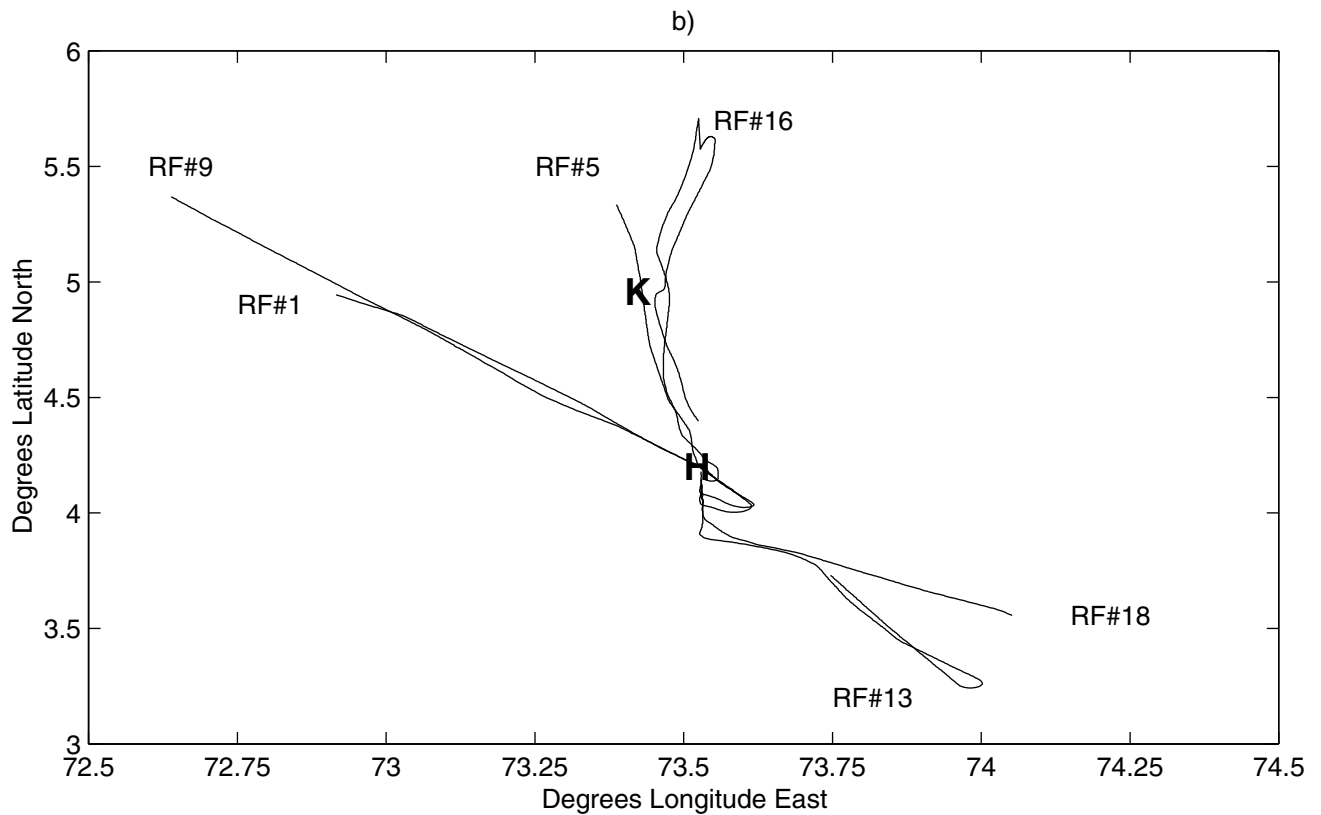
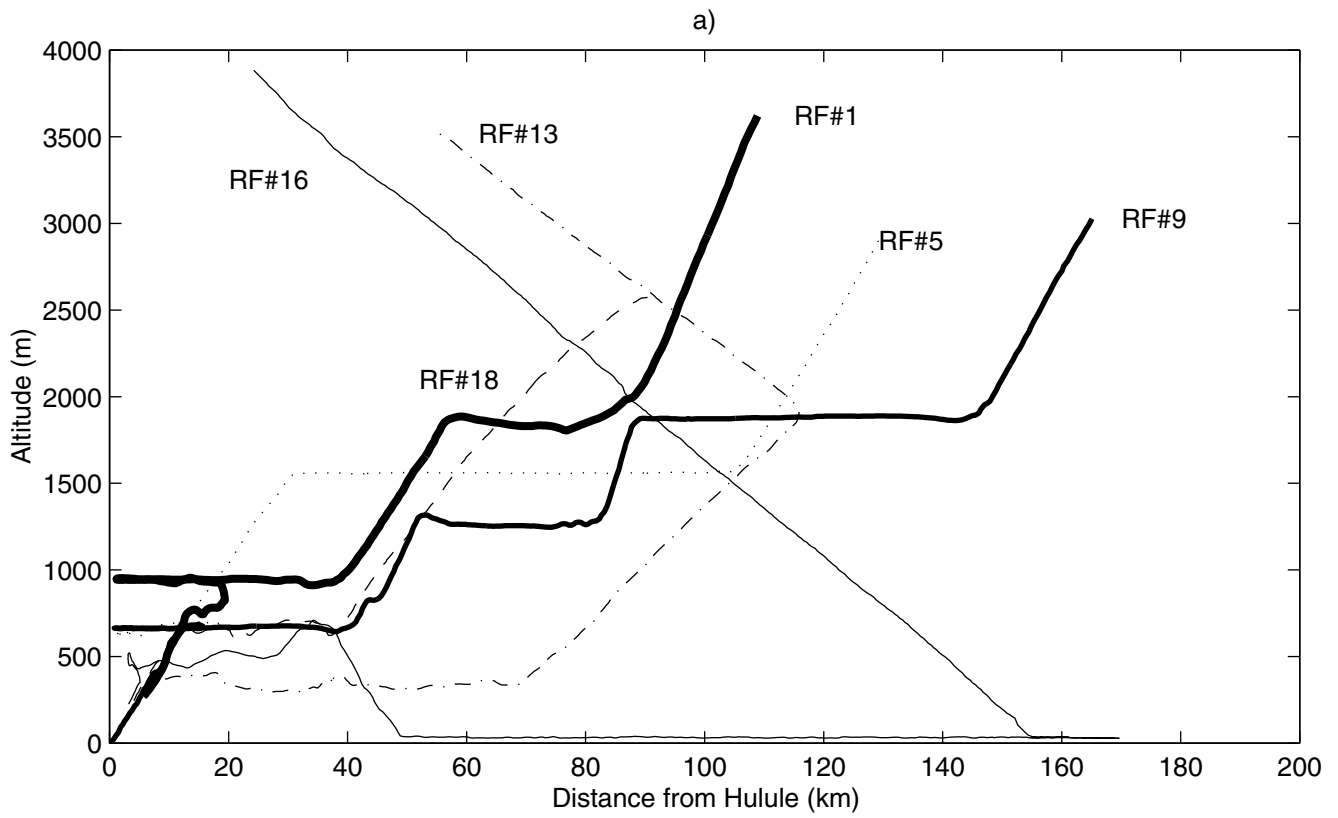


Figure 1.

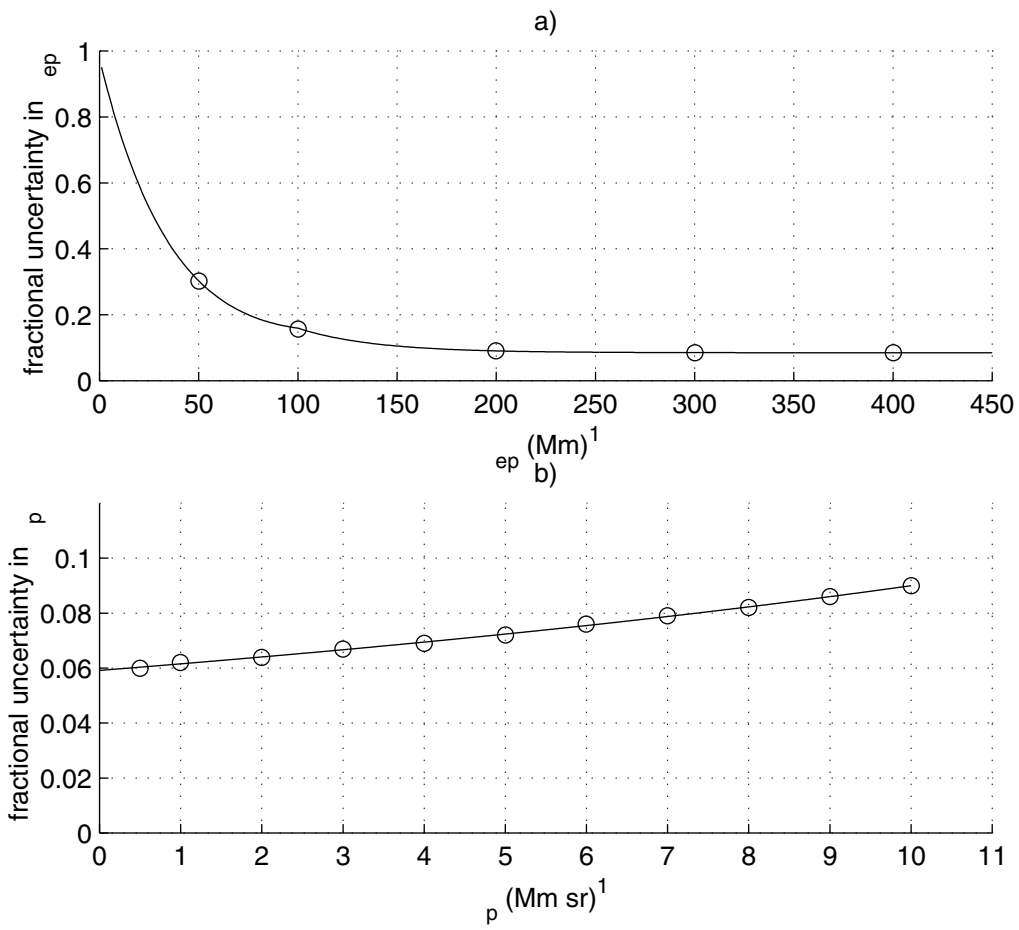
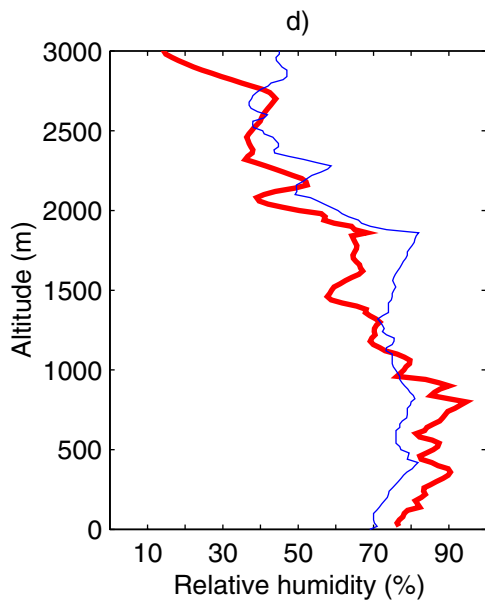
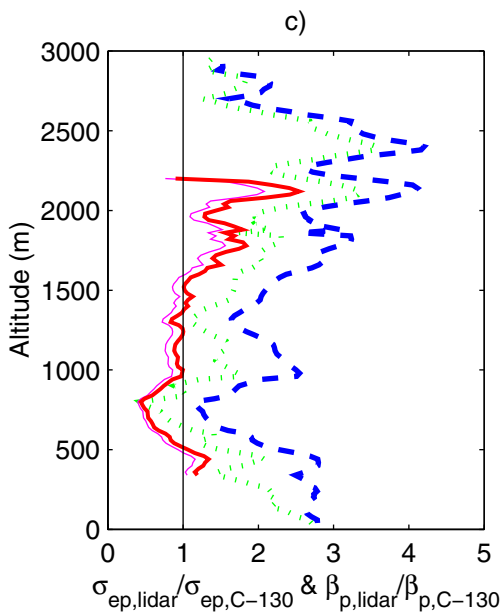
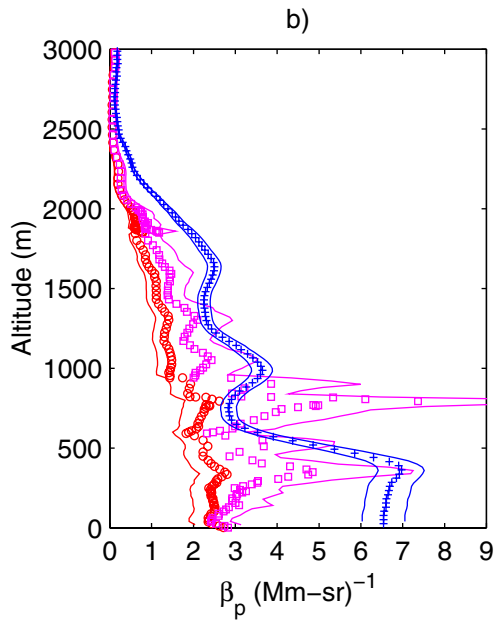
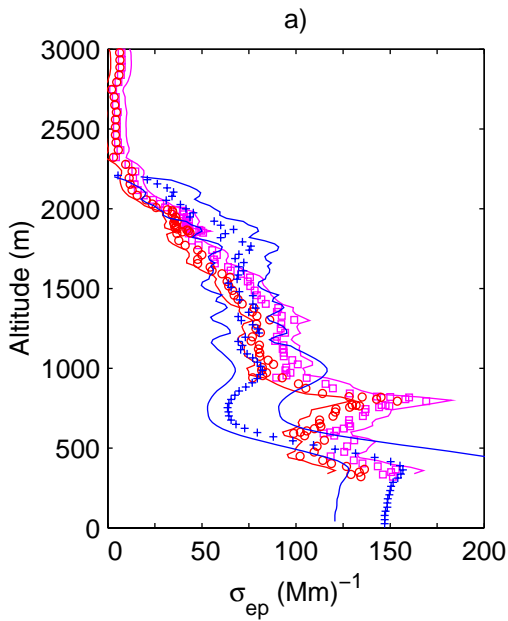
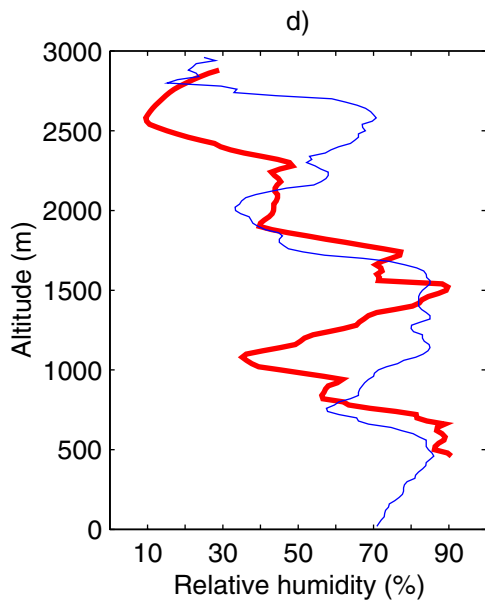
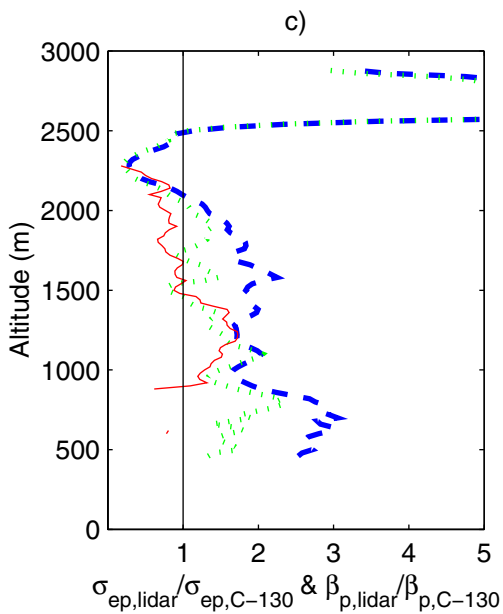
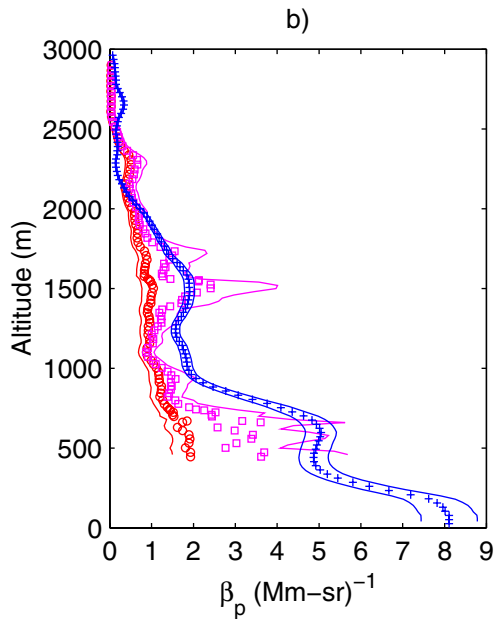
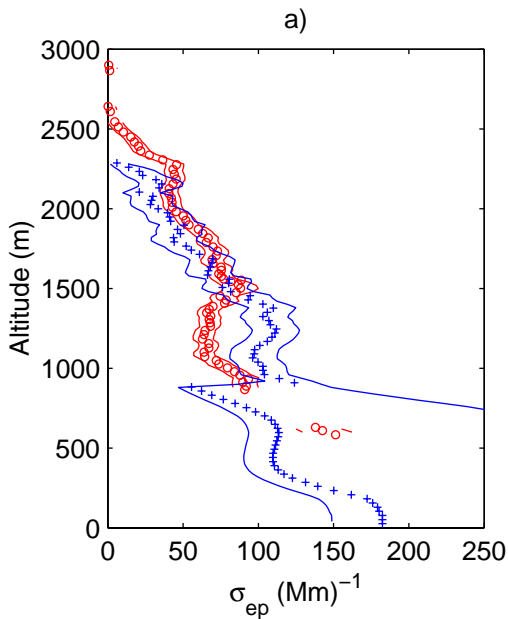
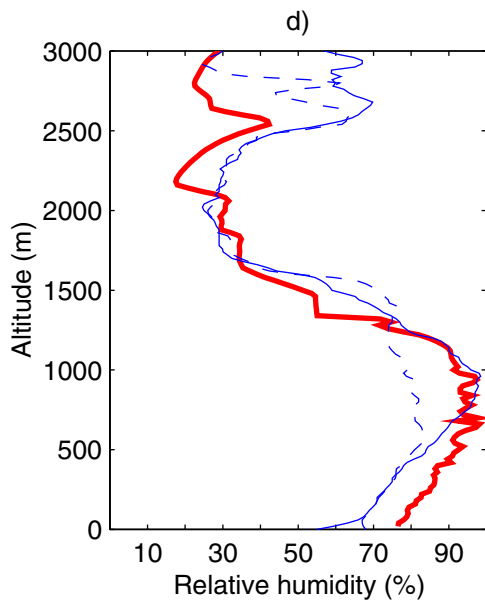
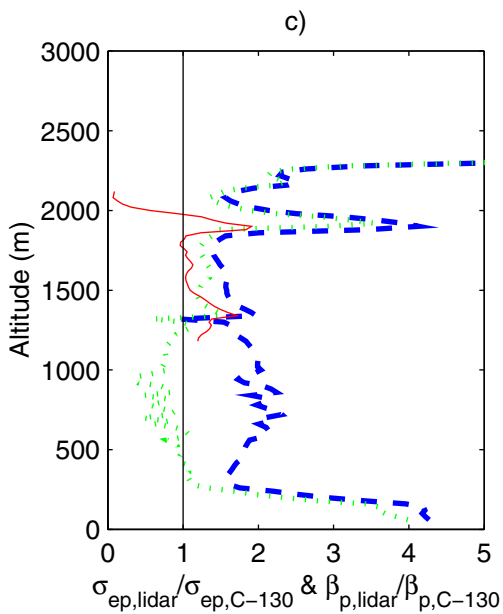
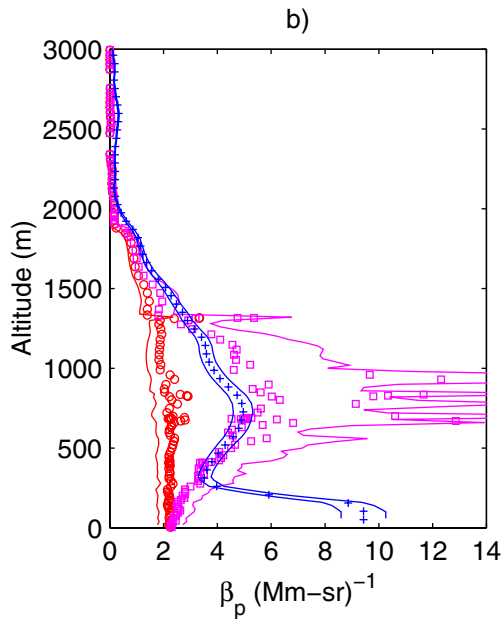
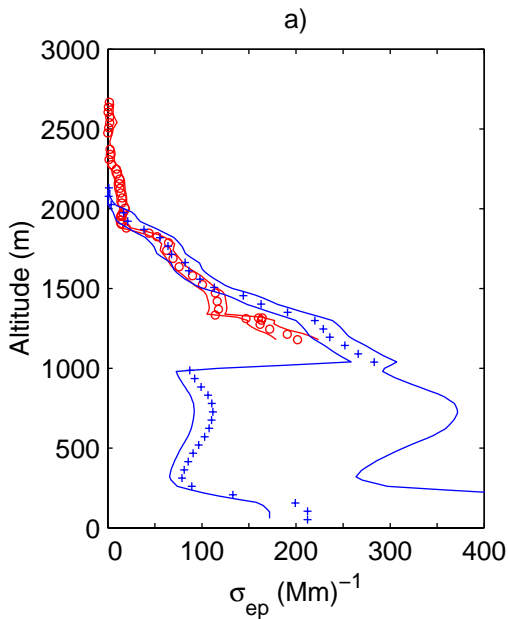
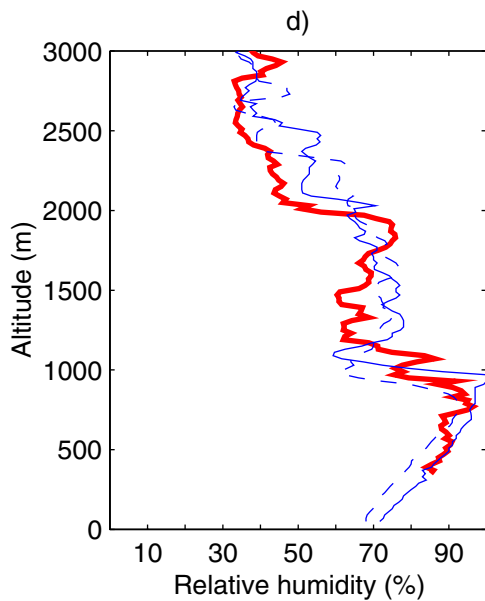
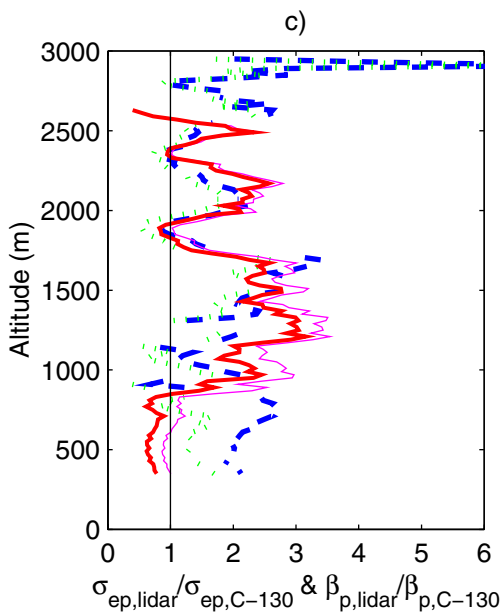
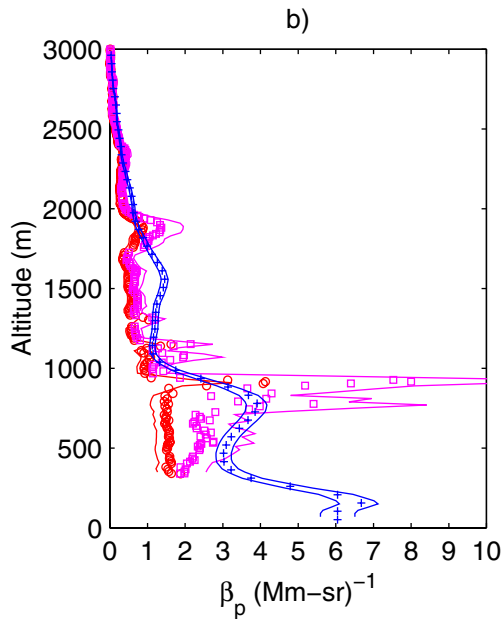
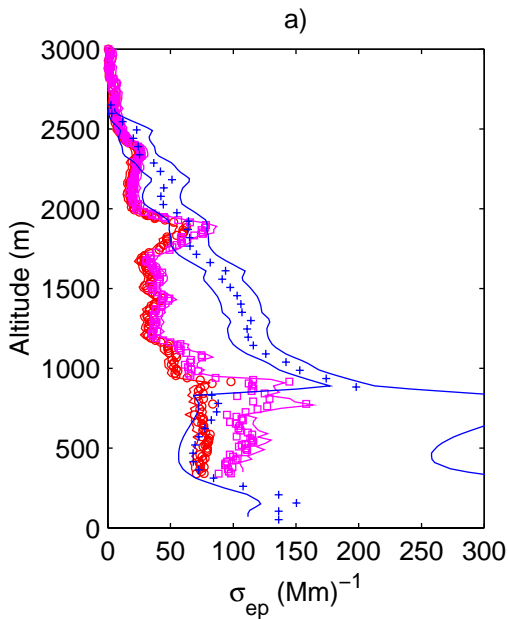


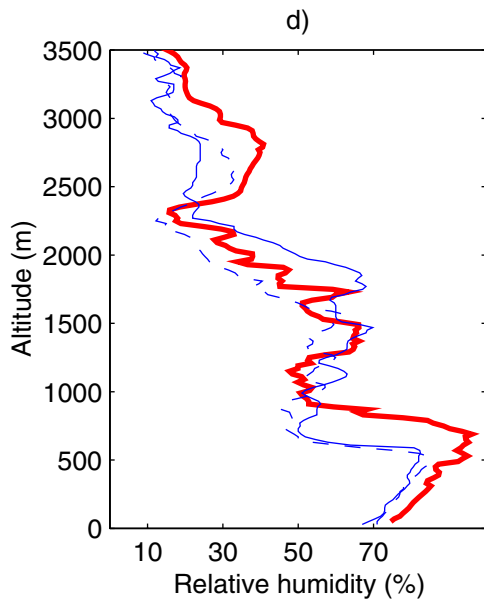
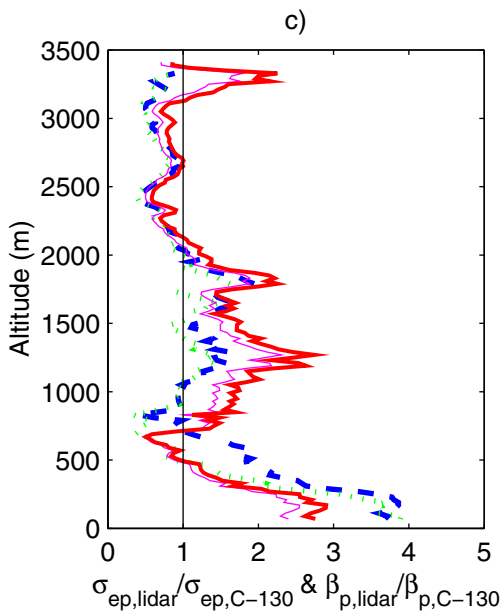
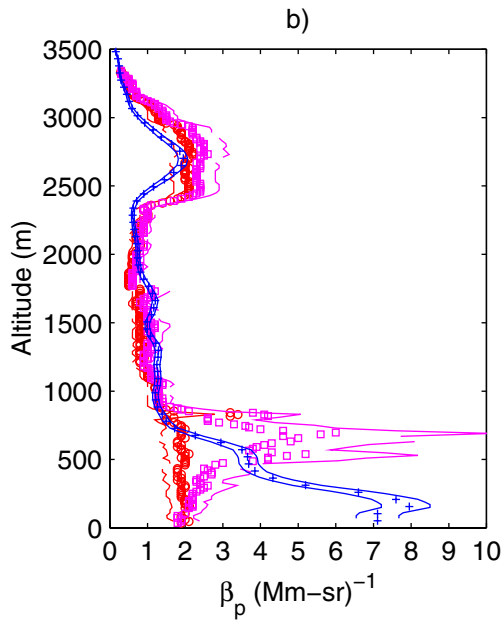
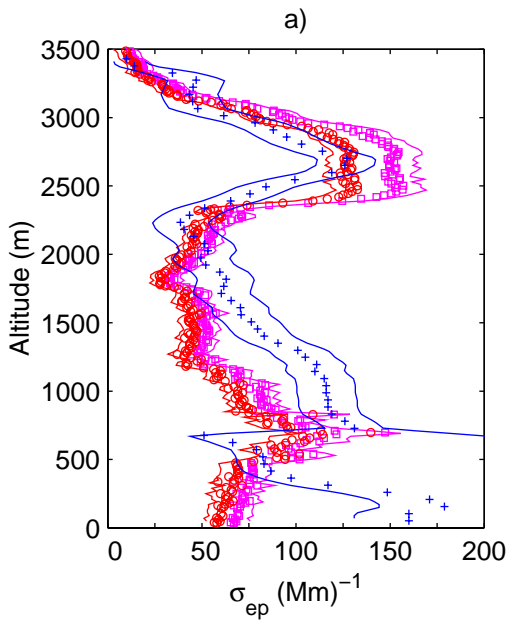
Figure 2.

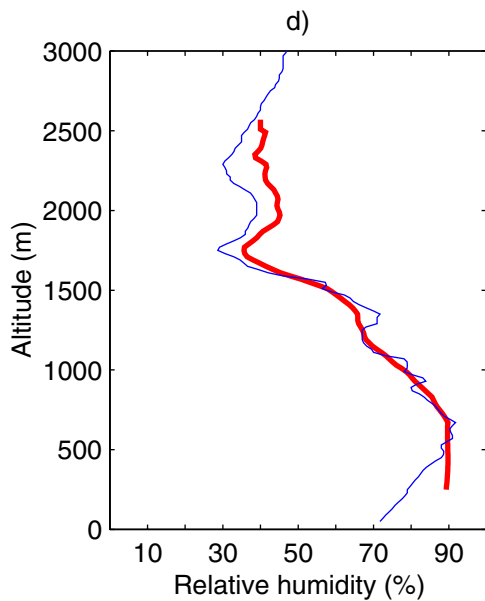
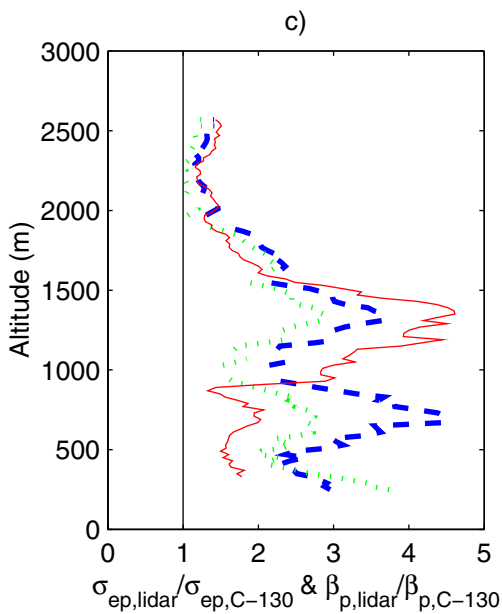
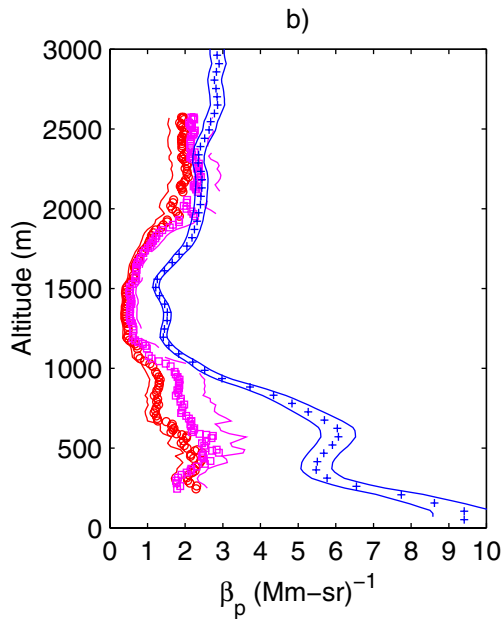
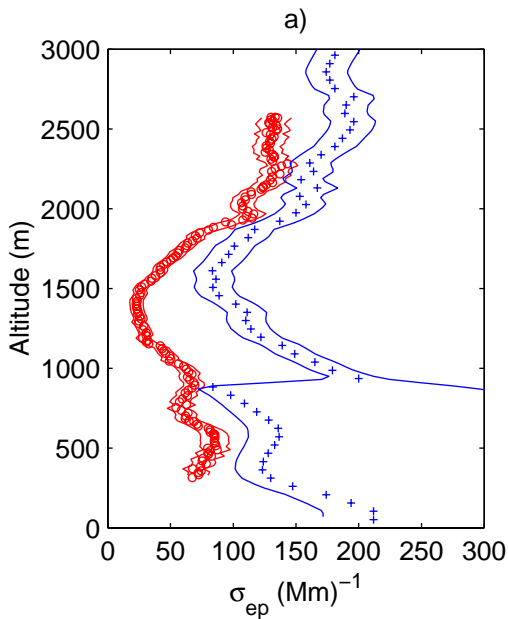


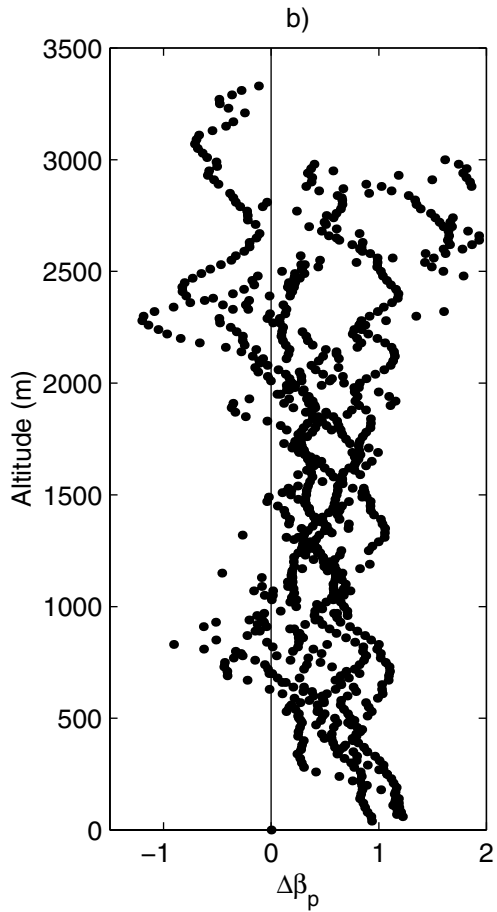
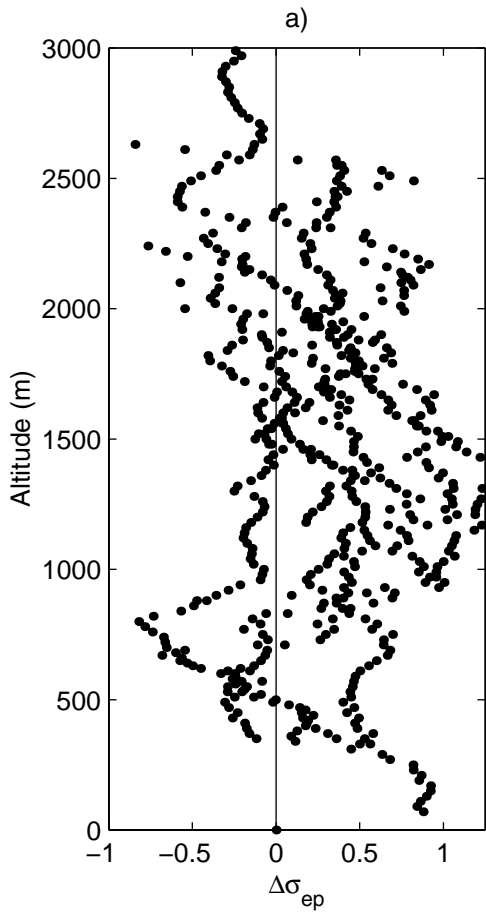


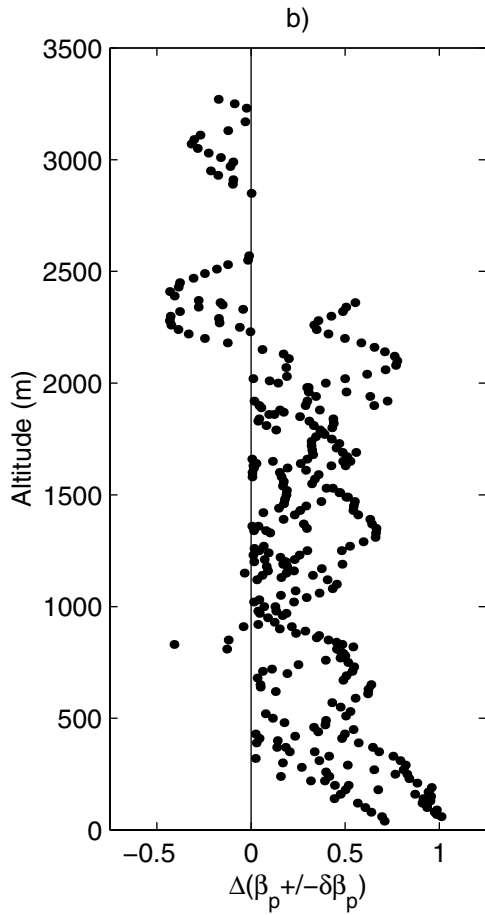
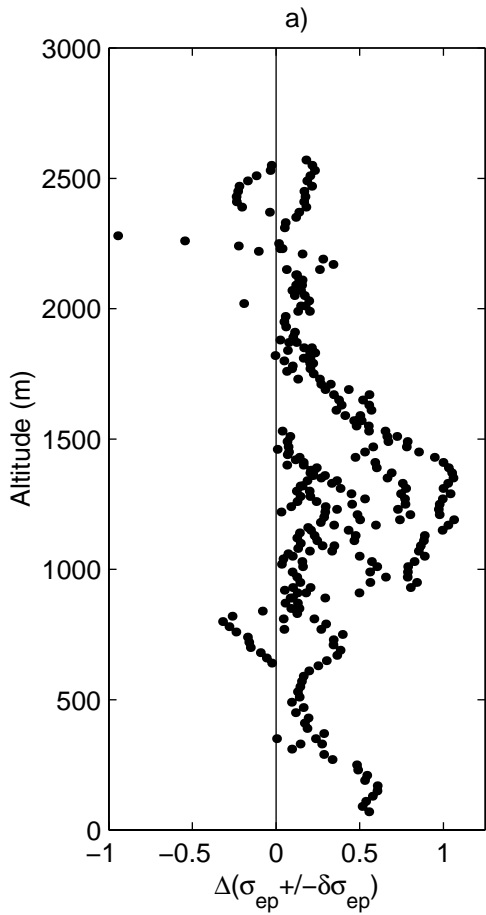












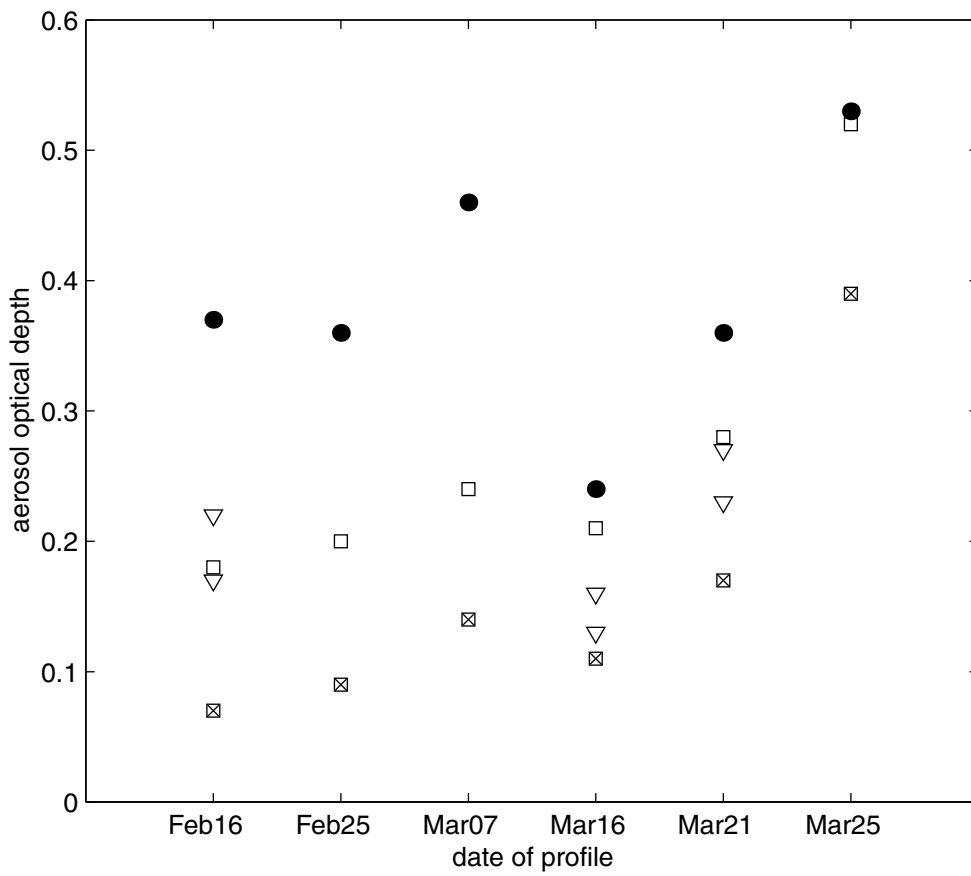


Figure 11.

